# The shape of fitness functions and the distribution of mutational effect sizes jointly limit adaptation by regulatory mutations

**Simon Aubé[1,2,3,4,5,6*], Alexandre K. Dubé[1,2,3,4,5] & Christian R. Landry[1,2,3,4,5,6*]**

1. Département de Biochimie, microbiologie et bio-informatique, Université Laval, 1045 Avenue de la Médecine, Québec, QC, Canada, G1V 0A6
2. Institut de Biologie Intégrative et des Systèmes (IBIS), 1030, Avenue de la Médecine, Université Laval, Québec, QC, Canada, G1V 0A6
3. PROTEO-Regroupement Québécois de Recherche sur la Fonction, l'Ingénierie et les Applications des Protéines, Université Laval, 1030, Avenue de la Médecine Québec, QC, Canada, G1V 0A6
4. Centre de Recherche en Données Massives de l'Université Laval, Université Laval, 1065, Avenue de la Médecine, Québec, QC, Canada, G1V 0A6
5. Centre de recherche en infectiologie, Université Laval, 2705 boul. Laurier, Québec, QC, G1V 4G2
6. Institut Intelligence et Données (IID), Université Laval, 2705 boul. Laurier, Québec, QC, G1V 4G2

**Correspondance: simon.aube.2@ulaval.ca and christian.landry@bio.ulaval.ca**

# Abstract

Mutations in gene regulatory regions have been shown to play a role in rapid adaptation but the factors determining their contribution are largely unknown. Using the yeast metabolic enzyme cytosine deaminase, we examine if adaptation to 5-fluorocytosine (5-FC), which requires reduced cytosine deamination and can readily arise from amino acid substitutions, may be reached by single promoter mutations. We generated all single-nucleotide substitutions and indels in the *FCY1* promoter and assayed the resulting mutants in presence of 5-FC. This revealed that no promoter mutation is sufficient for adaptation to occur. We next investigated how this inaccessibility of adaptation arises by combining large-scale expression measurements with the experimental characterization of the corresponding expression-fitness function. These experiments showed that the shape of this function precludes single promoter mutations from being adaptive. Although 24% of mutations significantly affect expression, the fitness curve is flat around wild-type level. As such, adaptation can only emerge from a severe reduction of expression, which cannot occur from a single mutation in the promoter. Our results show that the contribution of regulatory mutations to rapid adaptation not only depends on the distribution of mutational effect sizes on expression level but also on the shape of the function linking fitness to expression levels.

# Introduction

For rapid adaptation to occur, advantageous phenotypes must be immediately available through mutation. Whether a given mutation is adaptive depends on how the corresponding molecular change translates into a fitness effect. For expression changes, this is defined by the affected gene's fitness function (**Fig. 1a**) – describing the relationship linking expression level to organismal fitness –, of which a diversity of shapes have been reported[1]. As such, the corresponding distribution of mutational effects (DME) on expression level and the shape of the relevant fitness function jointly dictate if adaptive changes can arise within a given cis-regulatory region. These two factors thus have a major impact on the available pathways to adaptation, as well as on the rate and mode of regulatory evolution. Adaptation would for instance be unlikely to arise from the combination of a narrow DME, such that mutations have small effects on expression, with a step-like fitness function where only large expression changes are beneficial. Conversely, single-nucleotide mutations sampled from the same narrow DME could be adaptive if the fitness function instead displayed more gradual variation, allowing small expression changes to provide a benefit (**Fig. 1b**).

Fully understanding the evolution of cis-regulatory sequences and its contribution to adaptation hence requires assaying mutational effects on expression level and characterizing their conversion through fitness functions[2]. Previous large-scale studies have investigated the effect of mutations within promoters and cis-regulatory regions[3–9]generally focused on expression level without directly measuring the corresponding fitness consequences. Other studies collectively assayed the effects of cis-regulatory mutations on fitness and mapped the corresponding fitness function, for a limited number of yeast genes: *TDH3* [10–12] and *SUL1* [13,14]. As such, the interplay between the DME on expression level and the shape of the fitness function remains unknown for most genes, in spite of its prime importance for understanding the evolution of gene regulation [2]

Across organisms, a major engine of rapid adaptation is loss-of-function (LOF) mutations, both in coding and regulatory sequences. In humans, the best known mechanisms of resistance to malaria are the loss of expression of specific genes in red blood cells[15,16] and the partial loss of a key metabolic enzyme activity[17]. Among the best documented adaptive morphological changes in vertebrates in natural populations arose through the repeated loss of expression of a developmental gene[18]. LOF mutations in coding sequences are also a major pathway to antimicrobial resistance, for instance in fungal pathogens evolving in response to antifungal drugs[19]. Expression-decreasing epigenetic changes are involved in the adaptive evolution of cancer cells, by reducing expression of tumor suppressor genes[20]. Finally, laboratory microbial evolution has shown that adaptation occurs through LOF at least as frequently as through gain of function(s)[21–28]. LOF therefore provides a powerful model to investigate questions regarding the contributions of mutations to rapid adaptation.

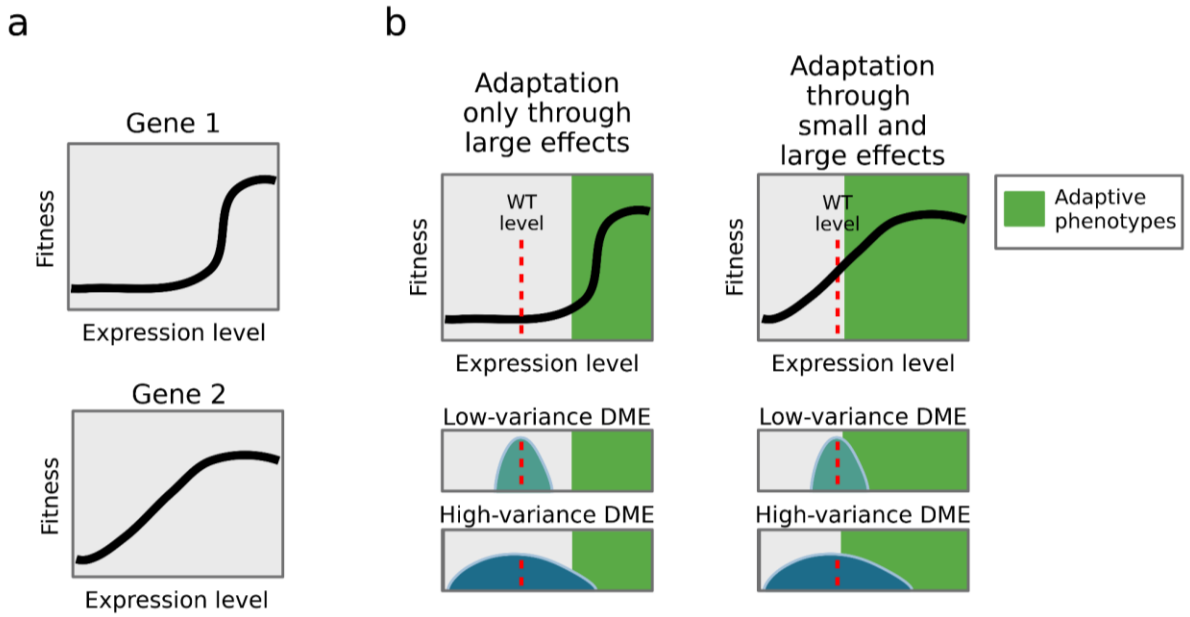


**Fig. 1: The DME and the shape of the fitness function jointly define the accessibility of adaptation. a,** Fitness functions describe the relationship between the expression level of a gene and organismal fitness. Hypothetical fitness functions are shown for two genes. In each case, the shape of the curve displays how fitness varies with increasing expression level of the corresponding gene. **b,** The accessibility of adaptation through expression level changes depends on mutational effect sizes and fitness function shape. For the two fitness functions, adaptation from the same low-fitness wild-type (WT) expression level is shown. When the function is flat around WT expression (left), only large expression increases from the high-variance DME can be adaptive. In contrast, when the fitness function is curved near WT expression (right), small expression increases are adaptive, such that adaptation is accessible from the low-variance DME as well as the high-variance one. Here, WT expression levels are shown to lie far from the high-fitness region for visual clarity. While such a situation is likely rare[1], the existence of beneficial gene duplications shows that it is possible[29–34]. Created in BioRender. Aubé, S. (2025) https://BioRender.com/rw8qljy.

We focused on the adaptive loss of Fcy1 activity in yeast exposed to prodrug 5-fluorocytosine (5-FC). While this enzyme's canonical activity is cytosine deamination, it also converts 5-FC into 5-fluorouracil, which leads to growth arrest and cell death[35]. Accordingly, complete or partial LOF mutations in the *FCY1* coding sequence confer resistance and are adaptive[36]. To assess whether regulatory mutations can also contribute to rapid adaptation to this condition, we performed saturation mutagenesis of the *FCY1* promoter. We measured the effect of all possible single nucleotide substitutions and indels in this region on fitness and expression level. These experiments revealed no measurable fitness gain in medium with 5-FC, although a quarter of single-nucleotide changes significantly affect gene expression level. Through the characterization of the underlying fitness function, we show that this discrepancy emerges jointly from the molecular effect of mutations and from the shape of this relationship. Because the fitness function is flat around the endogenous expression level, adaptation can only occur through large expression decreases,

which cannot arise from a single-nucleotide change in the promoter. These findings highlight how the availability of adaptative phenotypes through mutation can be restricted by the combined action of the DME and of the relevant fitness function. In *FCY1*, this results in rapid adaptation being only accessible through mutations in the coding sequence. This observation may be generalizable to other enzymes, especially those which exert low control over metabolic fluxes.

# Results

## Measuring the effects of mutations within the *FCY1* promoter

Because the growth of yeast *Saccharomyces cerevisiae* has been shown to decrease monotonically with increasing 5-FC concentrations[36] (**Fig 2a**, **Extended Data Fig. 1**), we hypothesized that at least some mutations in the *FCY1* promoter would be adaptive, by acting similarly as a decrease in the concentration of 5-FC (**Fig 2a**). To identify promoter regions to mutate, we performed deletions of successive 77 bp fragments of the intergenic region upstream of the *FCY1* gene. Among four tested deletions, only that of the most proximal fragment alleviated the toxicity of 5-FC **(Extended Data Fig. 2**). For this reason, and because most regulatory elements in yeast promoters are found within the 150 bp closest to the transcribed gene[37,38], we focused on the 154 bp immediately upstream of *FCY1*. Throughout, we defined nucleotide positions within this region relative to the start codon of *FCY1*, with position 0 assigned to the nucleotide immediately upstream of the gene and position -153 representing the nucleotide most distal from *FCY1*.

The mutagenized region corresponds to two fragments hereafter named F3 and F4 (**Fig. 2b**). Within each of them, we generated all single-nucleotide mutations – substitutions, insertions and deletions. The corresponding variants of F3 and F4 were inserted at the endogenous *FCY1* locus (YPR062W) using a CRISPR-Cas9-based pooled approach (**Fig. 2b**, *Methods*[39,40]). This resulted in 1021 unique mutated sequences (462 substitutions, 463 insertions and 96 deletions), of which 1020 were successfully recovered by sequencing of the mutant pools (**Supplementary Fig. 2**). This process was repeated four times for each of the three classes of mutations. The corresponding pools of substitutions, insertions and deletions were then combined (**Fig. 2c**), resulting in four independent transformation replicates, each containing all mutations. Because the set of substitutions was obtained by successively degenerating each nucleotide position, the WT *FCY1* promoter was also (re)constructed along with the desired mutants, at a frequency of ~17%.

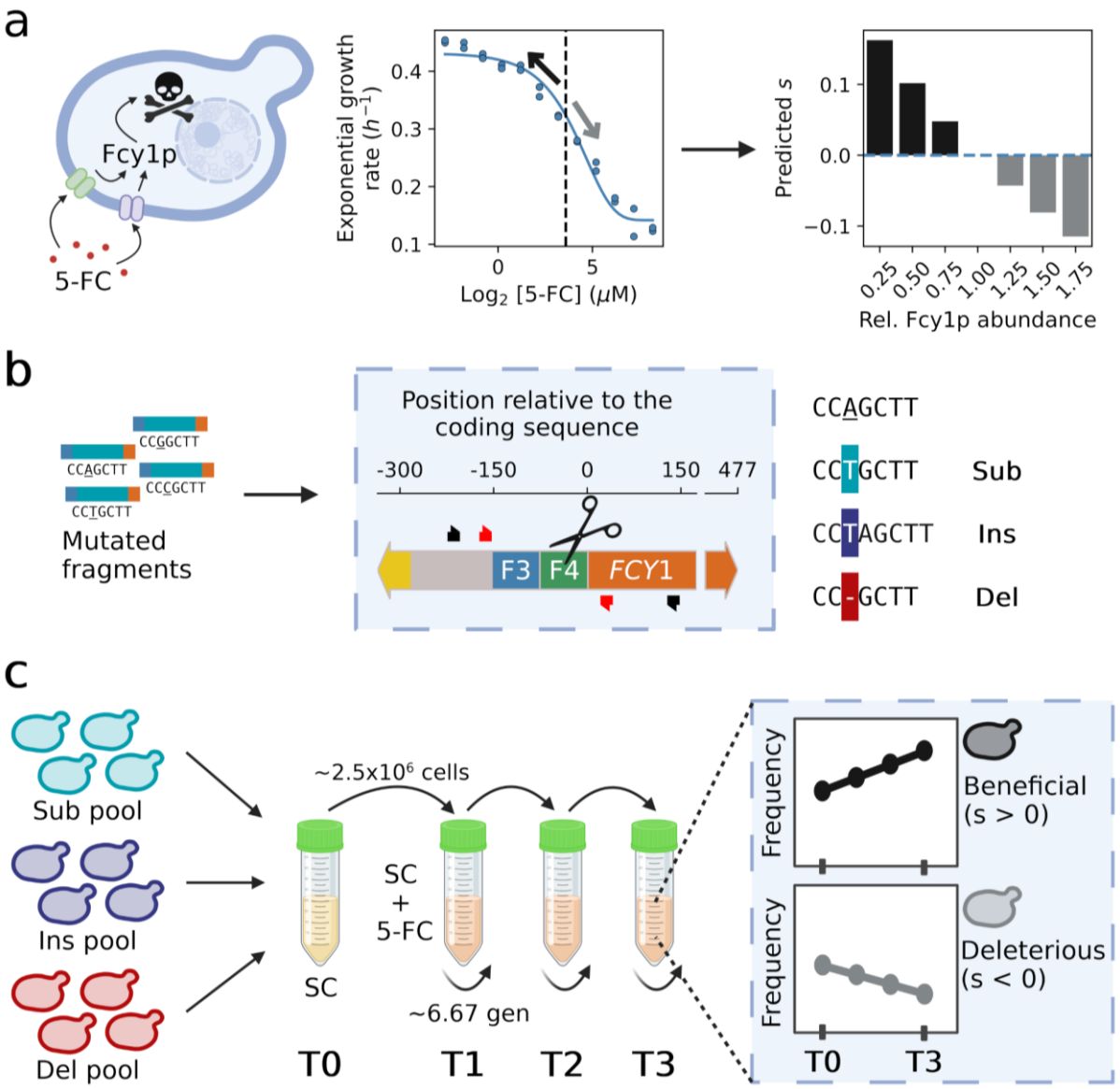


**Fig. 2: Assaying the accessibility of adaptation through single mutations in the *FCY1* promoter. a,** In presence of 5-FC, the activity of cytosine deaminase Fcy1 is toxic for yeast, by catalyzing the conversion of 5-FC into 5-fluorouracil. Accordingly, the growth rate of *S. cerevisiae* decreases with increasing 5-FC concentrations, as shown by the corresponding dose-response curve (**Extended Data Fig. 1a**). Under the naive assumption that changing the abundance of the Fcy1 protein is equivalent to varying the concentration of 5-FC, promoter mutations impacting *FCY1* expression could affect fitness. **b,** To generate mutated *FCY1* promoters, regions F3 and F4 (154 bp closest to the coding sequence) were replaced with libraries of synthetic sequences corresponding to all possible single-nucleotide substitutions (Sub), insertions (Ins) and deletions (Del). This was performed at the native genomic locus, using a CRISPR-Cas9-based method (*Methods*[39,40]). In downstream experiments, the various single mutants were genotyped by sequencing of the F3-F4 region, using oligonucleotide pairs shown in red (short fragment) and in black (extended fragment). **c,** The three types of mutant pools (Sub, Ins, Del) obtained from the genomic insertion of F3 and F4 variants were combined and grown in synthetic complete media (SC) and then transferred to media with 5-FC to allow for competition based on the abundance of Fcy1p. Loss of function of *FCY1* has no detectable effect in SC media without 5-FC.

At every timepoint, DNA was extracted and the edited locus was sequenced to follow the frequency of each mutant in the culture, allowing to estimate selection coefficient for each mutation from their enrichment or depletion through time. Schematics created in BioRender. Aubé, S. (2026) https://BioRender.com/k3mujqk.

From each of the four transformation replicates, two culture replicates were made, which were both grown in liquid media with [12 µM] 5-FC and without, resulting in 16 cultures. This concentration inhibits the growth of *S. cerevisiae* by ~50% and was previously used to assay all single-codon substitutions in the *FCY1* coding sequence[36] (**Fig 2a**, **Extended Data Fig. 1**). Additional replicates of all 16 cultures were also done by combining the promoter mutants with 960 representative coding sequence variants[36], to act as positive controls (**Extended Data Fig. 3**).

All 32 cultures were grown for ~20 generations in liquid media, with dilution every ~7 generations to maintain exponential growth (*Methods*). Samples were taken at each dilution step, as well as before the start of the experiment, resulting in a series of timepoints from T0 to T3 (**Fig. 2c**). The relative frequencies of all mutations were monitored by sequencing of the F3-F4 region (**Fig. 2b**) and the selection coefficient ($s$) associated with each promoter sequence was estimated from the slope of its log-scaled frequencies relative to the WT[41] (**Fig. 2c**).

Mutant pools sampled from the competition experiment were first genotyped by sequencing a 174 bp fragment, which covered the full F3-F4 region and the first 20 bp of *FCY1* (red oligonucleotide pair; **Fig. 2b**). There were however major reproducibility issues. While estimated selection coefficients were consistent between culture replicates of the same transformation, they diverged substantially across transformation replicates (**Supplementary Fig. 1a**). In addition, comparisons of the distributions of selection coefficients across the different time intervals revealed a gradual shift of the mean. From ~0 for the T0-T1 interval, it decreased below -0.15 for the full competition experiment (**Supplementary Fig. 1b**). Through further experiments, we found that these effects were caused by secondary mutations introduced during library construction (**Supplementary Fig. 1c-d**). We modified our sequencing protocol to genotype a longer region (black oligonucleotide pair; **Fig. 2b**) and repeated the analyses to eliminate these effects. We explain the observations in detail in the supplementary material (**Supplementary Note**) as we suspect these could be common in genome editing studies and thus be of broad interest.

## Fitness is robust to *FCY1* promoter mutations

After correcting for the impact of secondary mutations, the inferred selection coefficients for the F3-F4 mutants reveal only small fitness effects, which vary mostly uniformly along the mutagenized region (**Fig. 3a**). Across all assayed promoter mutations, median *s* estimates obtained from replicate experiments range from ~-0.037 to ~0.035 $gen^{-1}$, for a grand median of ~-0.002 $gen^{-1}$. Experimental noise moreover appears of a similar magnitude as these deviations from 0, as shown by an

226 average difference of ~0.028 $gen^{-1}$ between the highest and lowest *s* among replicate
227 estimates for the same genotype, up to ~0.110 $gen^{-1}$ (**Extended Data Fig. 4a**). A
228 small number of secondary mutations remain undetected (not found within the longer
229 sequencing fragment), resulting in outlier selection coefficients for one pair of culture
230 replicates within some F3-F4 genotypes. Following stringent removal of these rare
231 outliers (**Supplementary Fig. 8**), none of the 1020 *s* estimates for *FCY1* promoter
232 mutations appear significantly different from 0 ($p > 0.05$; one-sample t-test with
233 Benjamini-Hochberg correction at FDR=5%). Identifying significant effects using $|s|$
234 thresholds on the most extreme replicates instead results in small numbers of
235 significant changes (12 at $|s| > 0.01$), which are consistent with the null expectation
236 from random permutations of the data (**Extended Data Fig. 4**). Overall, we thus
237 conclude that there were no measurable fitness effects among the assayed single-
238 nucleotide mutations.
239
240 This absence of mutational effects is not due to a failure of the competition experiment,
241 as confirmed by two layers of controls. First, when considering all mutations (F3-F4
242 and secondary), the variance of estimated selection coefficients is indeed much
243 narrower for cultures without 5-FC (**Supplementary Fig. 9**). Second, selection
244 coefficients inferred for the added coding sequence mutants correlate well with
245 previously published variant effects[36] ($\rho = 0.780$ with $p < 10^{-64}$; **Extended Data Fig.**
246 **5a**). There is moreover almost perfect agreement between the two experiments
247 regarding the number and identity of resistance-conferring mutations (**Extended Data**
248 **Fig. 5b**). Together, these results confirm that adaptive changes would have been
249 observed in our assay, if they could occur through single-nucleotide promoter
250 mutations. We note that, whereas samples which contained coding sequence variants
251 also included the complete pool of promoter mutations (**Extended Data Fig. 3**), the
252 resulting cultures were not used to precisely estimate F3-F4 mutational effects.
253 Although noisier, the corresponding selection coefficients were nonetheless
254 qualitatively similar to those reported in **Fig. 3a** (**Supplementary Fig. 10**).
255
256 This absence of adaptive mutations within the *FCY1* promoter contrasts markedly with
257 the high accessibility of adaptation through changes in the corresponding coding
258 sequence. Within the *FCY1* gene, ~29% (408/1411) of single-nucleotide substitutions
259 indeed result in codon changes which confer resistance to 5-FC in the same conditions
260 (**Extended Data Fig. 5c**)[36]. Among these, only 67 introduce a premature stop codon.
261 As such, although adaptation to 5-FC is readily available through *FCY1* mutations, it
262 cannot be conferred by single-nucleotide changes in the promoter. In order to
263 understand how this inaccessibility of adaptation arises, we first measured the effect
264 of promoter mutations on *FCY1* expression.

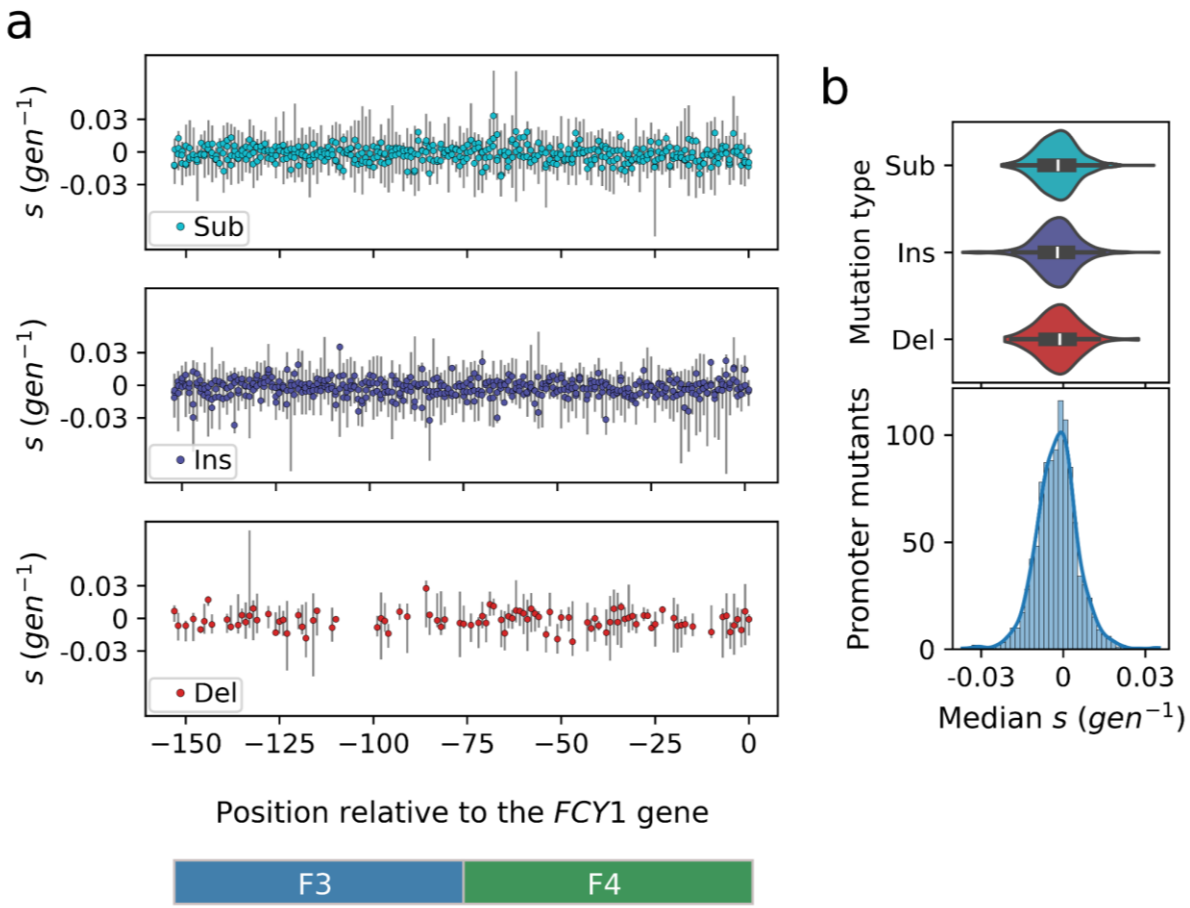


**Fig. 3: Mutations in the *FCY1* promoter do not have a measurable impact on fitness in 5-FC conditions. a,** Fitness effects of single-nucleotide mutations in the *FCY1* promoter. All substitutions (Sub; n=462), insertions (Ins; n=462) and deletions (Del; n=96) are shown. Points display the median selection coefficient for each mutant genotype, while error bars show the minimal and maximal values observed at each position along the mutated region. Nucleotide positions which appear to be missing are due to mutations which result in the same genotype (**Supplementary Fig. 2**), for instance deletion of any single base in a homopolymer region. Only data from two unbiased transformation replicates (each duplicated into two culture replicates; four samples in total) are shown (**Supplementary Note**, **Supplementary Fig. 6**). **b,** Distribution of mutational effects on fitness for single-nucleotide mutations in the *FCY1* promoter. The median selection coefficient obtained for each single mutant is shown, either as separate distributions for each of three classes of mutation (top) or as the full distribution (bottom; n=1020 observations, one per mutant).

## Many mutations in the *FCY1* promoter substantially affect expression level

To obtain expression level measurements for all promoter mutants, we used a sort-seq approach[42,43]. The complete pool of F3-F4 single mutants was reconstructed in a genetic background where the distal part of the *FCY1* gene – starting from its 43rd base – was replaced with a mEGFP sequence (*Methods*, **Extended Data Fig. 6**). As such, the translation initiation context could be maintained while adding a fluorescent

reporter to measure promoter activity. Yeast cells of the corresponding mutant library were sorted into five bins (numbered 0 to 4) according to their log-scaled fluorescence intensity (**Fig. 4a, Supplementary Fig. 11**). All the resulting samples were sequenced and read counts were used to compute a weighted average of bins for each genotype (*Methods*). The effect of each mutation was quantified using a $\Delta_{Ref}$ score equal to the difference between the corresponding mean bin and the average obtained for the WT. This was performed separately within each of six replicates (three transformation replicates, each subdivided in two culture replicates).

A narrow range of scores was obtained, with the median $\Delta_{Ref}$ of most promoter mutations falling between -1 and 0.5 (**Fig. 4b**). Of the 1020 F3-F4 mutants, 1019 were covered in at least two replicates after abundance-based filtering (*Methods*). Many secondary mutations were also recovered (**Fig. 4b**), including indels in the first 42 bp of *FCY1*. Interestingly, while most such mutations were associated with a low fluorescence intensity and thus a negative $\Delta_{Ref}$, some did not completely abolish expression. We specifically found out that indels which occurred before the second methionine codon of *FCY1* maintained ~10% of the WT fluorescence level (**Extended Data Fig. 7 a,b**). This is consistent with a previous report of a minor translation initiation site at this codon[44].

To validate the sort-seq assays, we selected 30 mutants for independent reconstruction (**Fig. 4b**). For each newly constructed strain as well as for the WT reference, fluorescence intensity was measured by flow cytometry (*Methods*). The resulting WT-relative intensities are in strong agreement with the corresponding median $\Delta_{Ref}$ scores (**Fig. 4c, Supplementary Fig. 12**). We additionally used this validation to draw up a calibration curve, enabling the conversion of sort-seq scores into more easily interpretable relative fluorescence intensities. To this end, we fit a LOWESS regression (**Fig. 4c**), to avoid making specific assumptions about the relationship between the two variables. This was performed within a bootstrapping routine which involved repeated resampling of $\Delta_{Ref}$ values as well as validation fluorescence measurements, thus generating 95% prediction intervals for the curve itself and for the relative fluorescence intensities of all genotypes (*Methods*, **Supplementary Table 9**). We hereafter refer to the medians of the latter intervals as WT-relative expression levels for the corresponding mutations, where a value of 1 denotes the WT level.

Examining the inferred relative expression levels for all F3-F4 mutants reveals a slight bias towards expression increases, with medians lying between 1.04 and 1.06 (**Fig. 4d**). That mutations are more likely to increase expression than to decrease it may appear surprising, since Fcy1p is already highly expressed and is among the 10% most abundant proteins in *S. cerevisiae*[45]. While this bias could be artefactual, the y-intercept of the calibration curve suggests otherwise (**Fig. 4c**). It is very close to 1

330 (∼1.00, with 95% prediction interval from 0.98 to 1.02) – as expected for a $\Delta_{Ref}$ of 0 –
331 , although no WT measurements were used in the LOWESS fitting.
332
333 The overall distribution of effects highlights that most single mutations in the *FCY1*
334 promoter impact expression levels by less than 15%, with 75% of variants lying
335 between values of 0.98 and 1.11 (**Fig. 4d**). Yet, we also observe a small number of
336 mutations with larger effects, decreasing expression to ∼50% of its WT level, or even
337 lower. This tail appears more pronounced than previously reported in yeast[3,49],
338 potentially because we specifically mutated the most proximal part of the *FCY1*
339 promoter, where mutations are more likely to disrupt processes such as transcription
340 initiation. Among the 1019 F3-F4 mutations, 245 significantly affect *FCY1* expression,
341 by 5% or more (95% prediction intervals). In agreement with a previous study of a
342 yeast promoter[13], these significant mutations are not distributed uniformly along the
343 mutagenized promoter region (**Fig. 4e**). This distribution reveals important
344 determinants of *FCY1* expression level.
345
346 The fact that significant mutations form two main clusters, from positions -132 to -127
347 (site 1) and from -125 to -120 (site 2), first highlights the importance of transcription
348 factor (TF) binding. Within these two sites, 92.4 % (73/79) of all variants change
349 expression by 5% or more, in a consistent direction within each cluster. Both sites are
350 within a 80 bp segment known to be critical for TF binding in yeast promoters[4,42,50],
351 while the whole -132 to -120 region is a hotspot of predicted TF binding sites[46] (**Fig.
352 4e top; Supplementary Table 10**). As such, the clusters likely reveal TF binding sites.
353 Interestingly, the deletion of either of the two sites is not more impactful than the
354 strongest mutations within the corresponding cluster (**Extended Data Fig. 8**),
355 suggesting that single mutations are sufficient to disrupt them.
356
357 The position of the two most impactful mutations additionally highlights how alterations
358 of transcription initiation may severely reduce *FCY1* expression. These variants, a
359 substitution and an insertion which respectively decrease expression to ∼16% and
360 ∼13% of its WT level (cytometry; **Fig. 4c**), both occur at position -9 (**Fig. 4e**). This
361 position is immediately downstream of the previously identified TATA-like element of
362 the *FCY1* promoter[47,48] – from -17 to -10 –, where the transcription pre-initiation
363 complex assembles. Additionally, the transcription of *FCY1* has been shown to initiate
364 at position -7[38,51]. The corresponding mutational effects thus likely reflect the disruption
365 of transcription initiation. The conflicting report of a most abundant transcript isoform
366 beginning further upstream, at -29[52], however adds uncertainty.

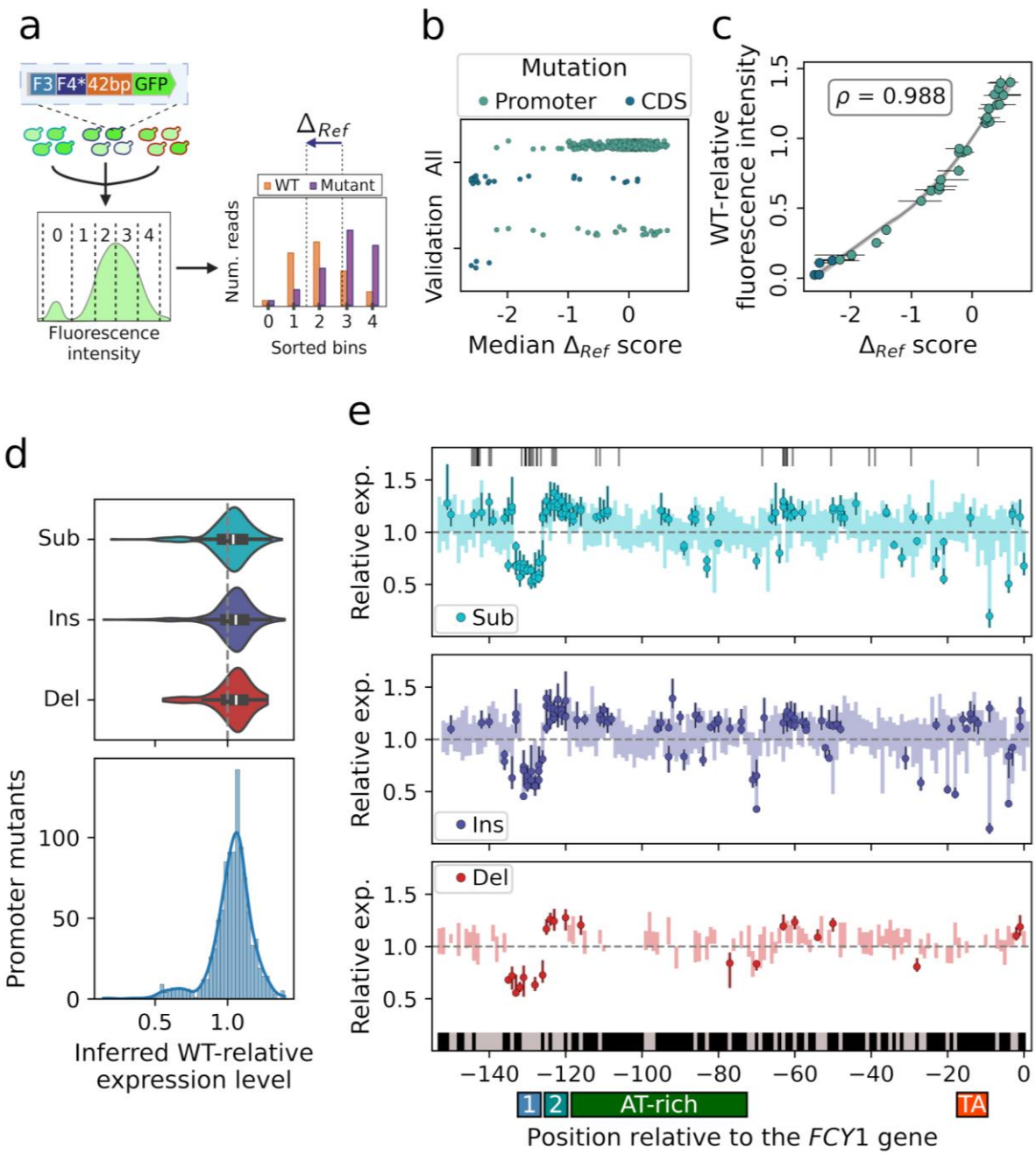


**Fig. 4: Mutations in the *FYC1* promoter impact expression level. a,** Schematics of the sort-seq experiment. Yeast cells from pools of promoter mutants were sorted into five bins according to their fluorescence intensity (representative distribution shown). From the sequencing of each bin, WT-relative fluorescence intensity could be estimated as a $\Delta_{Ref}$ score. Created in BioRender. Aubé,S. (2025) https://BioRender.com/uzzv5xy. **b,** Median sort-seq scores obtained for all variants detected across six replicate experiments. In addition to 1019 F3-F4 variants ("Promoter"), 28 single mutations in the first 42 bp of *FCY1* were identified ("CDS"), of which the vast majority are indels. The full distribution of scores ("All") as well as the 30 mutants selected for reconstruction ("Validation") are shown, split between the two categories in each case. **c,** Calibration curve of sort-seq scores**.** Points display the medians of sort-seq scores (n=6) and WT-relative fluorescence intensities (n=3) for all 30 validation genotypes. Horizontal and vertical error bars show the minimal and

maximal observations associated with each median. The high correlation between medians is shown with Spearman's rho ($p < 10^{-23}$). The line and the corresponding shaded area display a LOWESS fit with its 95% confidence interval (*Methods*). **d,** Distributions of WT-relative expression levels for all single-nucleotide promoter mutations, as inferred from the calibration of sort-seq scores. At the top, distributions are shown separately for substitutions (Sub; n=461), insertions (Ins; n=462) and deletions (Del; n=96), with a dashed line indicating WT expression level (1.0). At the bottom, the full distribution, combining all three types of single mutants, is shown (n=1019). **e,** Distribution of promoter mutations with a significant effect on expression (n=245), along the mutagenized region. Separately for Sub (n=113), Ins (n=111) and Del (n=21) variants, the estimated WT-relative expression (point) and its corresponding 95% prediction interval (error bar) are shown for each mutant affecting FCY1 expression by 5% or more (minimum or maximum of the corresponding 95% prediction interval; *Methods*). Shaded rectangles display the minima and maxima across all prediction intervals for each position along the sequence, including variants which are not shown. In the upper plot, vertical lines show the midpoint of hits (n=41) to known TF recognition motifs, identified using YeTFaSCo[46]. In the lower plot, the black and white rectangles respectively display A/T and G/C positions. Promoter positions corresponding with the two main clusters (sites "1" and "2"), the approximate AT-rich region and the TATA-like element ("TA")[47,48] are also identified.

Finally, the complete set of significant mutations underscores that most single-nucleotide changes within the poly(dA:dT) region of the *FCY1* promoter weakly affect its transcriptional activity. The corresponding AT-rich sequence, approximately between positions -118 and -73 (17.39% GC; **Fig. 4e**, bottom), is indeed comparatively depleted in strong mutational effects. Only 17.6 % (52/295) of variants within it are significant, compared to 26.7 % (193/724) in the remainder of the mutagenized region. This may seem contradictory, considering that such regions are important for the establishment of nucleosome-depleted regions within promoters[53,54], which favor transcription and can be sufficient to induce expression from a downstream core promoter[55]. It is however consistent with previous work on the *URA3* promoter, which showed that deletion of more than half of the corresponding 50 bp poly(dA:dT) was necessary to abolish expression[56].

Overall, we show that 24% (245/1019) of single-nucleotide mutations in the *FCY1* promoter have a significant effect on expression level, many of which appear to disrupt the binding of TFs at two putative sites. As such, *FCY1* expression is sensitive to mutations, meaning that the DME on expression level is not sufficient to explain the absence of fitness changes in 5-FC conditions.

## The expression-fitness relationship for *FCY1* is mostly flat

To investigate the mechanism underlying the absence of measurable fitness effects, we set out to characterize experimentally the expression-fitness relationship for *FCY1* (**Fig. 5a**). Six yeast promoters covering a wide range of expression levels were used to construct two sets of strains, in which each promoter was inserted upstream of either

426 the native *FCY1* sequence or the previously described 42bp-mEGFP construct
427 (**Extended Data Fig. 6c**). The *FCY1* strains were grown in media with 5-FC (12 μM;
428 like in the competition experiment) – to obtain growth rate measurements –, while
429 mEGFP strains were used to measure expression levels (*Methods*). For each
430 promoter, the measurements from the two strains were combined to draw the
431 corresponding expression-fitness curve (**Fig. 5a**).
432

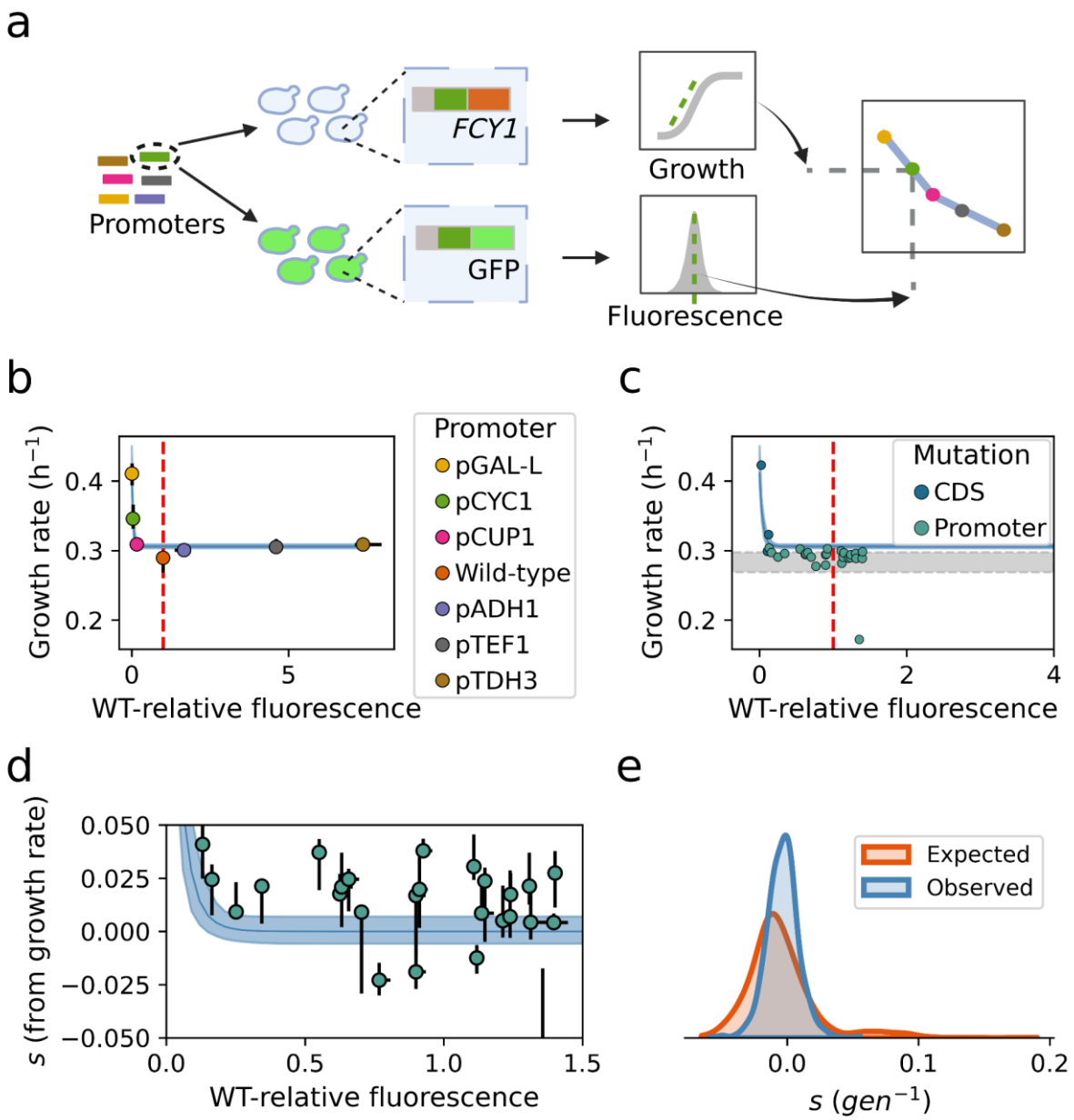


433
434 **Fig. 5: The *FCY1* expression-fitness function is flat around WT expression level,**
435 **making fitness robust to promoter mutations. a,** Strains with varying expression
436 levels were constructed to measure the fitness function. A set of yeast promoters
437 covering a wide range of activities were introduced in the genome in place of the
438 endogenous *FCY1* promoter, either upstream of *FCY1* or of a fluorescent reporter.
439 Created in BioRender. Aubé, S. (2025) https://BioRender.com/1p60mp7. **b,**
440 Expression-fitness relationship for *FCY1* in 5-FC conditions. The four promoter

441 constructs expressing *FCY1* to at least ~18% of its WT level display very similar growth
442 rates. For each promoter, medians of growth rate and WT-relative fluorescence (n=3)
443 are shown along with the corresponding minima and maxima (error bars). The fitness
444 function is displayed as a fitted exponential decay function, with its corresponding 95%
445 confidence interval (*Methods*). The WT strain, which lacks a resistance cassette and
446 is not directly comparable to the other ones (*Methods*), was not used in the fit. **c,**
447 Growth rates of reconstructed mutants are consistent with the fitness function. For
448 validation mutants (**Fig. 4c**) which could also be reconstructed in the *FCY1*
449 background, medians (n=3) are shown for growth rates in 5-FC [12μM] media and WT-
450 relative fluorescence intensities. This includes single promoter mutations ("Promoter";
451 n=26) and indels in the first 42 bp of the gene ("CDS"; n=3). The dashed line identifies
452 the WT expression level (1.0), while the shaded area displays the range of growth rates
453 measured for the WT background (panel **a**), into which the mutations have been
454 reconstructed. **d,** Reconstructed promoter mutations are mostly neutral. For the same
455 set of single mutations in the promoter (n=26), medians (n=3) are shown for selection
456 coefficients and relative fluorescence intensities, with error bars displaying the
457 corresponding minimal and maximal replicates. Selection coefficients are computed
458 from growth measurements (*Methods*) shown in the previous panel, relative to the WT
459 strain. The previously fitted fitness function (panels **b** and **c**) is displayed with its
460 corresponding 95% confidence interval, after conversion into selection coefficients.
461 Only the region of the expression-fitness curve where promoter mutants lie is shown.
462 The outlier mutant which is hidden is associated with a median *s* of ~-0.28. **e,** The
463 shape of the fitness function prevents expression changes from affecting fitness. The
464 DME on fitness observed in the competition experiment is much narrower than the one
465 expected from the relationship between the concentration of 5-FC and growth rate
466 **(Fig. 2a**, **Extended Data Fig. 1**).
467
468 This experiment revealed a very steep fitness function, where growth rate decreases
469 sharply until *FCY1* expression reaches ~18% of its WT level and then plateaus (**Fig.**
470 **5b**). Consequently, this fitness curve is flat around the WT, such that small expression
471 changes have no fitness effect. The shape of this function is thus consistent with the
472 fact that no single-nucleotide promoter mutation conferred resistance to 5-FC in our
473 bulk competition experiment. To further validate this result, we leveraged previously
474 characterized validation mutants. The set of alleles used in the calibration of sort-seq
475 measurements, which also includes a small number of indels in the coding sequence,
476 was reconstructed in the native *FCY1* background and the resulting strains were
477 phenotyped in 5-FC conditions (*Methods*). In combination with the corresponding
478 relative fluorescence intensities, these growth measurements confirm the flatness of
479 the curve around WT expression level. Almost all promoter mutants display WT-like
480 growth rates, with no clear trend along the complete range of effects (**Fig. 5c**). Among
481 three assayed coding sequence mutations, the only one which reached the high
482 fitness region is associated with a ~98% decrease in fluorescence intensity
483 (**Supplementary Table 11**), caused by a frameshift-inducing indel. This highlights how
484 adaptation is only possible through very large reductions in Fcy1 abundance, which
485 cannot be achieved by single promoter mutations. Zooming in on the promoter
486 mutants further illustrates this point. Among them, the two single mutations with the

largest effect barely reach the threshold below which fitness rapidly increases, although they respectively decrease *FCY1* expression to ~16% and ~13% of its WT level (**Fig. 5d**). As such, the shape of the fitness function, jointly with the corresponding DME, renders adaptation to 5-FC inaccessible from single changes in the *FCY1* promoter.

The flatness of the fitness function around WT expression contrasts markedly with the steepness of the 5-FC dose-response curve around the 12 μM concentration used (**Fig 2a**, **Extended Data Fig. 1**). If varying the abundance of Fcy1p instead had the same effect as changing the 5-FC concentration, large fitness differences would have been observed among the set of promoter single mutants. The most impactful mutation, decreasing Fcy1p abundance to ~13% of its WT level, would have been associated with a *s* of 0.19, while seven other mutations would have resulted in $s > 0.1$ (**Fig. 5e**). Adaptation would then have been accessible through regulatory changes, albeit much less readily than from mutations in the coding sequence.

Whereas growth rate varies according to 5-FC concentration, the shape of the fitness function remains mostly constant. Across concentrations resulting in ~10% to ~70% inhibition for the WT, growth rate variation is restricted to the same narrow range of relative expression levels and only the height of the corresponding plateau varies (**Extended Data Fig. 9a**). A similar phenomenon is observed in media lacking uracil, where the deamination of cytosine into uracil by Fcy1p is essential for growth. With increasing concentrations of cytosine, the height of the plateau of high fitness increases, while the region of varying fitness remains mostly the same (**Extended Data Fig. 9b**). At 5-FC and cytosine concentrations resulting in similar levels of relative inhibition or growth, the fitness functions obtained in the two conditions are very similar, with a sign inversion (**Extended Data Fig. 10ab**). This suggests that our results also extend to the canonical cytosine deaminase function of the Fcy1 enzyme. Growth measurements for a set of promoter mutants covering the full range of mutational effects confirm that increasing *FCY1* expression, as allowed by the DME of single mutations, is not adaptive under uracil starvation (**Extended Data Fig. 10c**). Overall, these experiments demonstrate that adaptation is not accessible from single-nucleotide changes in the *FCY1* promoter, in LOF (5-FC) as well as in gain-of-function (cytosine) contexts. This is due in part to the small number of large mutational effects on gene expression, but more importantly to the shape of the fitness function, which is flat around WT expression level.

# Discussion

The rapid accessibility of adaptive changes through regulatory mutations depends on their effect sizes on gene expression and on the relationship between fitness and expression level. One powerful approach to investigate these determinants is to focus on a gene where adaptation is known to arise and systematically assay all single regulatory mutations. To this end, we studied the promoter of the gene *FCY1*, a

530 protein-coding region within which single-nucleotide changes have been shown to
531 confer resistance to the drug 5-FC[36,57]. We show that no promoter mutation has a
532 measurable fitness effect in yeast exposed to this molecule, although large changes
533 in expression level (reaching a reduction of 87%) are observed. In this adaptive
534 landscape, beneficial phenotypes are thus inaccessible from single nucleotide
535 variation in the promoter, although they arise readily from mutations in the
536 corresponding coding sequence[19,36].
537
538 Our initial data instead suggested that most promoter mutations were highly
539 deleterious. Further investigations revealed that this result was due to secondary
540 resistance-conferring mutations introduced during library construction, outside of the
541 sequenced region (**Supplementary Note; Supplementary Fig. 1,4-8**). These
542 beneficial mutations largely occurred in the WT promoter background, since this
543 genotype was generated at high frequency within the mutant pool. This comparatively
544 made all true promoter single mutants appear less fit. Interestingly, bias thus arose
545 from the reconstruction of the WT within the CRISPR library, which is widely regarded
546 as a best practice to ensure the accuracy of mutant fitness estimates[58]. Such artifacts
547 may be common in large-scale genome editing experiments, due to the increased
548 frequency of single-nucleotide mutations – and especially indels – in synthetic DNA
549 oligonucleotides[59]. This highlights the importance of designing library construction
550 workflows which minimize the use of genic regions as homology arms to guide
551 recombination. Alternatively, these segments should at least be fully included in the
552 genotyping region, as we did to correct our experiment.
553
554 Within our *FCY1* model system, the inaccessibility of adaptation through promoter
555 mutations emerges jointly from the shape of the fitness function and from the DME on
556 expression level. Whereas the fitness function is flat around WT protein abundance,
557 single promoter mutations do not push expression level far enough to escape this
558 fitness plateau. A related phenomenon has been observed for the *TDH3* gene of *S.*
559 *cerevisiae*, for which the effects of cis-regulatory mutations on expression and fitness
560 have been extensively studied[10–12,49,60]. A vast majority (216/235) of single mutations
561 in the *TDH3* promoter were reported to lie on a plateau of the fitness function and thus
562 have no significant effect on fitness[10]. Yet, because the deletion of *TDH3* only
563 decreases fitness by ~5%[10,12], the relevance to adaptation is unclear. For *FCY1* in 5-
564 FC conditions, a 30-40% fitness increase is in contrast possible through LOF
565 (Extended Data Figs 2, 7). Similarly, the characterization of 1400 single-nucleotide
566 substitutions in the *SUL1* promoter of *S. cerevisiae* revealed only 61 mutations
567 significantly affecting fitness, with the largest reported increase approaching 10%[13]. In
568 this case, cis-regulatory mutations were assayed in conditions where *SUL1* coding
569 mutations and copy number amplifications can respectively increase fitness by 23%[61]
570 and 51%[33]. While this is more directly comparable to *FCY1* in 5-FC, the corresponding
571 DME on expression level was not measured and the fitness function was only partially
572 characterized[14]. As such, it is difficult to assess whether the paucity of fitness effects
573 among mutants of the *FCY1*, *TDH3* and *SUL1* promoters emerges from similar

574 mechanisms. More studies characterizing additional promoters as well as the
575 corresponding fitness functions are needed.
576
577 Although data on multiple cis-regulatory regions is currently lacking, dissecting how
578 the absence of adaptive mutations in the *FCY1* promoter arises still offers clues
579 regarding the generalisability of this observation. An important caveat is however that
580 this model may not represent a typical gene. Because the same loss of expression
581 which allows adaptation to 5-FC also impedes the canonical cytosine deaminase
582 activity (**Extended Data Figs 9, 10**), the inaccessibility of LOF-based adaptation
583 through promoter mutations may reflect past selection to improve this latter function.
584 This is suggested by the high abundance of Fcy1p, in the top 10% among yeast
585 proteins[62], which could have arisen by progressively climbing up the increasing fitness
586 curve observed in cytosine conditions (**Extended Data Fig. 9**). Such an evolutionary
587 trajectory would imply that the apparent plateau of the fitness function actually displays
588 a small curvature, visible to natural selection but not measurable using our
589 experimental approach[63]. As such, the *FCY1* model may be representative only of
590 adaptive pathways which involve the loss of a previously optimized function. It
591 nonetheless provides a useful framework to understand how and under which
592 conditions adaptation may occur through a single cis-regulatory mutation. An
593 additional caveat is that we have only assayed the adaptive potential of *FCY1* mutants
594 under constant 5-FC exposure. It is plausible that, in a fluctuating environment where
595 the concentrations of 5-FC and cytosine would both vary, adaptation could occur
596 through cis-regulatory mutations.
597
598 In the current study, the absence of adaptive mutations in the *FCY1* promoter first
599 arises from the rarity of mutations strongly decreasing expression. This is largely
600 consistent with previous work, and thus likely to apply to a number of other genes. The
601 large-scale mutagenesis of promoters and regulatory elements in yeast[3,49] and
602 mammals[6–9] indeed showed that only a minority of single mutations strongly affect
603 expression. In the yeast *TDH3* promoter, for instance, only 7.7% (18/235) of mutations
604 were reported to decrease expression by more than 6%[49], compared with 17.2%
605 (175/1019) in the *FCY1* promoter (**Fig. 4d**). Moreover, genome-scale computational
606 predictions indicate that 10% of cis-regulatory mutations account for 50% of
607 expression variation in yeast[4]. The DME on expression level we report is thus likely
608 representative of many yeast genes, although larger changes could potentially have
609 been observed if indels of variable lengths[64] had been included. The *FCY1* promoter
610 is in addition a typical yeast promoter. It is TATA-less like the majority of such
611 regions[47,65], features the most common poly-T/poly-A configuration[54] and belongs to
612 the most abundant class of yeast promoters (2474/5378)[66]. Whereas it is bidirectional,
613 it drives higher expression of *FCY1* than of the opposite gene and there are hundreds
614 such promoters in the yeast genome[67].
615
616 Second, the saturating shape of the *FCY1* fitness function prevents even the most
617 impactful promoter mutations from affecting fitness. Such abundance-fitness curves

618 featuring a plateau have generally been reported for enzymes across organisms[1,68–
619 72], including the well-studied *TDH3* of *S. cerevisiae*[10,12]. They are additionally expected
620 from enzyme kinetics and metabolic control theory[63,69]. In the case of *FCY1*, the
621 flatness of the fitness function around WT expression was unexpected from the steep
622 growth response to changes in 5-FC and cytosine concentrations (**Extended Data**
623 **Fig. 1**). This suggests that permeases, rather than the Fcy1 enzyme, may be exerting
624 control over metabolic flux. A similar phenomenon has been reported in bacteria, with
625 the β-galactosidase enzyme and the corresponding permease. While the former
626 displays a step-like fitness function as *FCY1*, the latter is associated with a much more
627 graded fitness function, such that small activity or abundance changes may have
628 selective consequences[70]. More generally, recent proteomics and metabolomics
629 studies have shown that, in most cases, changing the abundance of a single yeast
630 enzyme has a weak impact on the corresponding metabolic flux[73–75]. Overall, it thus
631 appears likely that the shape of the *FCY1* fitness function emerges from fundamental
632 principles. As such, it is plausible that LOF-based adaptation is similarly inaccessible
633 from single mutations in the cis-regulatory regions of a substantial number of other
634 enzymes, in yeast but potentially also in other organisms.
635
636 Contrary to promoter mutations, single-nucleotide substitutions in the *FCY1* coding
637 sequence readily confer adaptation to 5-FC[36] (**Extended Data Fig. 5**). In accordance
638 with the fitness function we report (**Fig. 5b**), this would mean that 29% (408/1411) of
639 coding mutations decrease the abundance or activity of the Fcy1 enzyme below 5%
640 of its WT level. This mutational accessibility is consistent with numerous other studies
641 showing that a substantial fraction of missense mutations in protein sequences induce
642 LOF[68,76–83]. The contrast with single mutations in the *FCY1* promoter, among which
643 the most impactful decreases expression to 13% of its WT level, is nonetheless
644 striking. If large-effect mutations are generally rare in cis-regulatory regions – as is the
645 case for *FCY1*, *TDH3*[10,12,49] and *SUL1*[13] in yeast –, LOF-based adaptation would then
646 largely occur through coding changes. Whether coding mutations contribute
647 predominantly to adaptation, including in gain-of-function contexts, remains a fully
648 open question. Two recent surveys of adaptive mutations, in yeast evolved across
649 different environments[28] and in pathogenic fungi exposed to diverse antifungal
650 drugs[19], have collectively identified only tens of adaptive noncoding changes,
651 compared with thousands of coding mutations. Yet, a large fraction of these mutations
652 are LOF-inducing. Single promoter mutations conferring adaptation have moreover
653 been identified across bacteria[84–86], yeast[87] and humans[15,16] and have even been
654 associated with a reduction of expression in some instances[15,16,85,87]. Fitness
655 differences between two yeast strains have in addition previously been attributed
656 largely to noncoding variants[88]. As such, elucidating whether coding or regulatory
657 mutations generally contribute more to adaptation will likely require additional
658 experiments as well as a systematic literature comparison similar to that of Hoekstra
659 & Coyne[89].
660

Recent work demonstrates that it is now possible to comprehensively assay the effect of mutations in full-length promoters, even in multicellular organisms[91]. An important complement to such work should be the characterization of the corresponding fitness functions. In *FCY1*, its step-like nature makes promoter mutations much less impactful on fitness than expected (**Fig. 5e**). More generally, an important role for fitness function shape in defining whether cis-regulatory or coding mutations contribute more to adaptation was previously theorized from data on a handful of mutations conferring β-lactam resistance in bacteria[90]. When the WT resides on a fitness plateau, as is the case for *FCY1*, expression changes are unlikely to provide a large fitness benefit (**Fig. 6a**). Coding mutations, on the other hand, may cause complete LOF – like in our *FCY1* model – or bypass the fitness plateau by modifying the curvature of the fitness function (in gain-of-function contexts), for instance by changing the affinity of an enzyme for its substrate[90]. When the WT instead resides in a region of the curve where fitness varies rapidly, expression variation provided by regulatory mutations could be equally beneficial as coding changes (**Fig. 6b**). An additional possibility, suggested by the discrepancy between cis-regulatory and coding effects on Fcy1p abundance, would be that, in case of a peaked fitness function, regulatory mutations could be favored due to large-effect coding changes (e.g. LOF) overshooting the optimum (**Fig. 6c**).

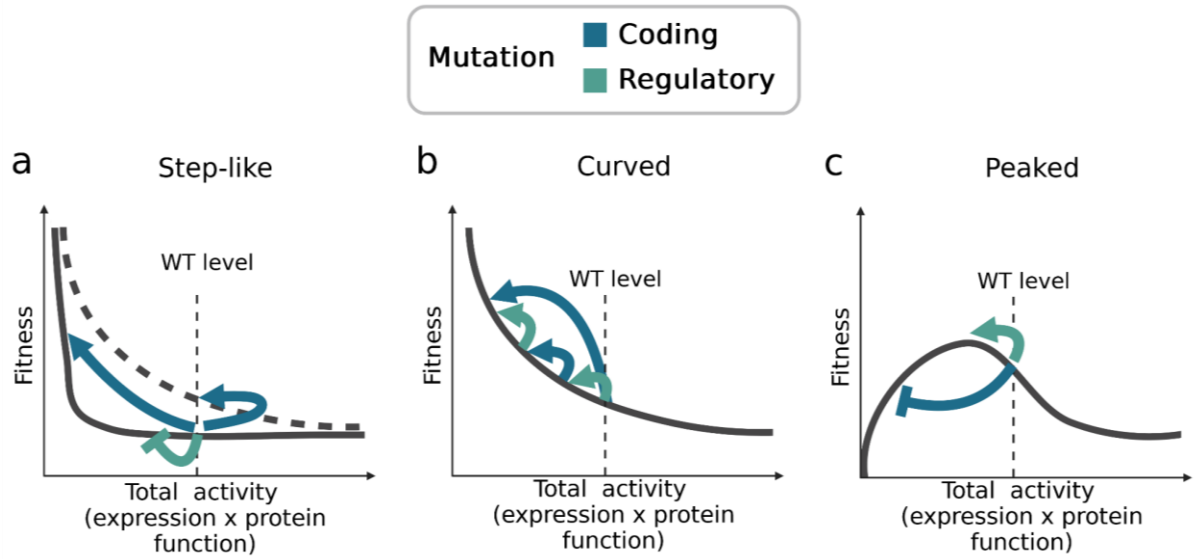


**Fig. 6: Different shapes of fitness function may favor rapid adaptation through cis-regulatory or coding changes.** Although we only measured expression level for *FCY1*, fitness functions are here generalized to total protein activity. For consistency with our experiments, all three are drawn under the assumption that a decrease in activity provides a benefit. **a,** A step-like fitness function where the WT lies on a plateau, far from the fitness cliff, would favor mutations inducing complete LOF or modifying the fitness curve through functional changes in the protein[90]. If LOF cannot occur through a single cis-regulatory mutation, as we report for *FCY1*, this type of mutation will not be selected for (blunt arrow). **b,** A fitness function with high curvature around WT would allow a wide range of mutational effects to provide a benefit. LOF mutations, as well as cis-regulatory or coding changes with more moderate effects on activity, may all be selected for. **c,** A non-monotonic fitness function would favor smaller changes in total activity. Because they overshoot the curve's optimum, LOF-

693 inducing mutations would be deleterious and accordingly selected against (blunt
694 arrow). If such large effects were only found among coding mutations, cis-regulatory
695 changes could be comparatively favored. Created in BioRender. Aubé, S. (2026)
696 https://BioRender.com/ksrv5jw.
697
698 Altogether, previous studies and our results demonstrate the importance of
699 considering the shape and curvature of fitness functions to understand the molecular
700 bases of adaptation. Jointly with the DME on expression level and other molecular
701 traits, fitness functions dictate the availability of adaptive changes. Through
702 widespread characterization of mutational effects and expression-fitness
703 relationships, the breadth of adaptive pathways available in different contexts may be
704 better understood, revealing whether major trends exist among genes or every gene
705 is idiosyncratic. This importance of shape and curvature goes beyond the relationship
706 between fitness and expression levels in microbes, as it appears key for phenotypic
707 traits in general. For instance, it was recently shown that considering the full shape of
708 gene dosage response curves significantly enhances our understanding of genotype-
709 phenotype relationships in humans[92].
710

711 # Methods

712 ## Strains, oligonucleotides, plasmids and culture media

713 All *S. cerevisiae* strains constructed in this study were generated from a BY4742 (*his3Δ leu2Δ*
714 *lys2Δ ura3Δ*) background[93] harboring a hygromycin resistance marker at the *HO* locus
715 (*hoΔ::HPHMX*). This AKD1123 parental background and all other strains are listed in
716 **Supplementary Table 1**, along with the identity of the corresponding genomic inserts and
717 PCR primers as well as the selective media used. The sequences and references for all
718 oligonucleotides used in this study can be found in **Supplementary Table 2**, while references
719 for all plasmids are listed in **Supplementary Table 3**. Recipes for culture media are detailed
720 in **Supplementary Table 4**. When specified, selective media was prepared by adding one or
721 multiple of the following agents: geneticin [200 µg/mL] (G418; Bioshop Canada),
722 nourseothricin [100 µg/mL] (NAT; Jena Bioscience) and hygromycin B [250 µg/mL] (HYG;
723 Bioshop Canada). All Sanger sequencing was performed at the sequencing platform of Centre
724 de recherche du CHU de Québec-Université Laval (Université Laval, Québec, Canada).
725

726 ## Yeast transformation

727 Whenever inserts which included a selection marker had to be inserted in the yeast genome,
728 a standard lithium acetate yeast transformation protocol was used[94]. After selection of
729 transformants on the appropriate selective media, four to eight clones were selected for
730 validation PCR, depending on the strain. Unless stated otherwise, colony PCR was performed
731 on each side of the integration site to confirm proper integration, using Taq polymerase
732 (Bioshop Canada). All genomic inserts were amplified using the KAPA HiFi HotStart DNA
733 polymerase (Roche Molecular Systems).
734
735 This approach was for instance used to delete each fragment F1 to F4 of the intergenic region
736 between *JID1* (*YPR061C*) and *FCY1* (*YPR062W*), as well as the full intergenic segment and
737 the complete *FCY1* region (including the corresponding gene), by the insertion of a *natNT2*
738 cassette[95]. This resulted in a set of six strains harboring a different deletion of the *FCY1* region

739 (SA0127, SA0128, SA0129, SA0130, SA0131, SA0132). Similar deletions of regions F3 and
740 F4 were also performed in the 42bp-mEGFP construct obtained by CRISPR-Cas9 yeast
741 transformation (see below), generating fluorescent strains SA0246, SA0247 and SA0254
742

743 ## CRISPR-Cas9 yeast transformation

744 When sequences needed to be inserted in the yeast genome without any flanking selection
745 marker, a CRISPR-Cas9 approach was used. This required the prior generation of a strain
746 harboring a *natNT2* cassette at the chosen insertion site, which was done through standard
747 yeast transformation as described above. Competent cells from this genetic background could
748 then be cotransformed with the pCAS-NAT plasmid (**Supplementary Table 3**) – encoding a
749 guide RNA engineered to target the Cas9 endonuclease to the *natNT2* cassette[39] – and the
750 desired repair DNA, amplified with KAPA HiFi HotStart DNA polymerase (Roche Molecular
751 Systems). A previously published CRISPR-Cas9 transformation protocol was followed[96].
752 Briefly, competent cells were prepared as described, and transformed with unpurified PCR
753 amplification of the insert, DNA carrier [10 mg/ml], pCAS-NAT and PLATE solution
754 (polyethylene glycol 2000 [40%], lithium acetate [0.1 M], Tris-EDTA [10 mM Tris-Cl, 1 mM
755 EDTA] buffer [pH=8.0]). After mixing, cells were incubated for 30 minutes at 30°C, heat
756 shocked for 15 minutes at 42°C, resuspended in YPD media and incubated for 4-6 hours at
757 30°C. Transformation reactions were plated on YPD media containing G418, to select for
758 uptake of the pCas plasmid, and incubated at 30°C for 48 hours. Eight colonies from each
759 transformation were then grown overnight (30°C with shaking) in liquid YPD and streaked on
760 solid YPD. After 48 hours of incubation at 30°C, one isolated clone from each streaking was
761 grown overnight in YPD (30°C with shaking) and spotted on both YPD and YPD+G418 solid
762 media, to confirm the loss of the pCAS plasmid. Because the AKD1123 parental background
763 is resistant to hygromycin, HYG was added to the YPD throughout. Correct integration was
764 then validated by colony PCR and Sanger sequencing.
765
766 Using this protocol, the reinsertion of deleted regions F2, F4 and F1-F4 (full intergenic) was
767 performed, resulting in strains SA0162, SA0166 and SA0170. It was also used to generate
768 the 42bp-mEGFP construct (SA0228) to measure *FCY1* expression level and all validation
769 clones expressing either *FCY1* or mEGFP from the *FCY1* locus.
770

771 ## Growth assays

772 Unless stated otherwise, the following protocol was used each time the growth of *FCY1* strains
773 was assessed in media containing 5-FC (Alfa Aesar) or cytosine (Alfa Aesar). Each yeast
774 strain of interest was first inoculated in three replicates in SC [pH=6] liquid media – potentially
775 with HYG, NAT and/or G418, depending on each strain's resistance marker(s) – and grown
776 overnight at 30°C with shaking. After ~16 hours of incubation, a sample (100 µl) of each culture
777 was centrifuged and resuspended in the same volume of sterile water, before being aliquoted
778 and diluted again in sterile water to obtain up to 250 µl of cells at 1 optical density (OD) unit/ml.
779 Growth assays were then assembled in Greiner flat-bottom transparent 96-well plates as
780 follows: 160 µl of media (SC complete for 5-FC or SC-Ura for cytosine); 20 µl of diluted cells
781 [OD=1]; 20 µl of 5-FC or cytosine diluted to obtain the desired final concentration in a volume
782 of 200 µl. Each plate was incubated for 48 hours at 30°C without shaking in a Tecan Infinite
783 M Nano (Tecan Life Sciences) and $OD_{595}$ was measured at 15 minutes intervals.
784

785 To obtain exponential growth rates, the exponential part of each growth curve was first
786 identified. The end $T_{max}$ of the exponential phase was defined as the time where the derivative
787 of OD, estimated as the moving median of differences between consecutive OD
788 measurements, reached its maximum. To limit experimental noise, the first two hours of OD
789 measurements were discarded, while any $T_{max}$ above 30 hours or below 3 hours was ignored.
790 In such cases, the first ten hours of the growth curve were instead defined as the exponential
791 phase. Exponential growth rates were then estimated as the slope of the linear regression of
792 $log(OD)$ over time. When converting the growth rate of any strain $i$ into selection coefficient
793 $s_i$, the following formula was used[97]:

$$s_i = \frac{\mu_i - \mu_{WT}}{\mu_{WT}} \log 2$$

794
795 Variables $\mu_i$ and $\mu_{WT}$ are the growth rates for the strain of interest and the corresponding WT
796 reference, respectively. This comparison was always made using WT measurements obtained
797 in the same experiment as the growth rate of strain $i$.
798

799 ## Construction of the mutant libraries

800 **Amplification of mutated F3 and F4 promoter fragments**

801 All single-nucleotide substitutions, insertions and deletions in the F3 and F4 regions were
802 ordered as six separate oPools Oligo Pools (Integrated DNA Technologies Inc.) containing
803 sequences of 117 bp, 118 bp and 116 bp, respectively. Within the different pools, each
804 oligonucleotide is a variant of the full-length F3 or F4 region (77 bp) with flanking 20 bp
805 homology regions at both ends. The latter sequences are respectively the 20 bp immediately
806 upstream or downstream of the corresponding fragment in the reference genome of *S.*
807 *cerevisiae* S288C, as retrieved from the Saccharomyces Genome Database[98]. For
808 substitutions, each position of each fragment was iteratively degenerated into all four possible
809 nucleotides by specifying a N base, while for insertions, the same mixed base was inserted in
810 3' of each position in the reference F3 and F4 sequences. When such a N is encountered, an
811 equal ratio of each of the four standard nucleotides (A, T, G, C) is dispensed during synthesis.
812 For the two pools of deletions, single-nucleotide removal was performed iteratively at each
813 position of F3 and F4 and duplicates (occurring whenever two or more consecutive nucleotides
814 are identical in the reference) were removed to obtain non-redundant sets. All sequences
815 ordered as part of the six oPools are listed in **Supplementary Table 5**.
816
817 Upon reception, each oPool was spun down and resuspended in fresh PCR-grade water, to
818 obtain a final concentration of 50 µM. Aliquots of 100 µl at 0.05 µM were then obtained by
819 serial dilution from 2 µl of the initial resuspension. From these aliquots, PCR amplification of
820 each oPool was performed in four replicates using KAPA HiFi HotStart DNA polymerase
821 (Roche Molecular Systems) and the following cycle: 98°C for 3 min; {98°C for 30 s; 60°C for
822 15 s; 72°C for 10 s} x 22; 72°C for 20 s; Hold at 10°C. Each reaction was done in 50 µl:

| Volume (µl) | Reagent |
|---|---|
| 33 | PCR-grade water |
| 10 | KAPA HF buffer [5X] |
| 1.5 | dNTPs [10 mM] |
| 1.5 | Forward oligo [10 µM] |
| 1.5 | Reverse oligo [10 µM] |
| 1.0 | KAPA Hi-Fi HotStart DNA polymerase |
| 1.5* | oPool [0.05 µM] (or PCR-grade water) |
| **50** | **Total** |

823 In each case, the diluted oPool resuspension was not added to the reaction mix and was
824 instead added individually in each reaction tube. In addition, one control without the oPool
825 dilution was performed for each primer combination. Both primer pairs were designed to
826 extend the 20 bp homology regions included in the oPool, such that mutated F3 and F4
827 featured 60 bp homology arms upstream and downstream of the corresponding genomic
828 region. The two pairs were CLOP299-C3 / CLOP299-C4 and CLOP299-D3 / CLOP299-D4,
829 respectively to amplify F3 and F4 oPools.
830
831 **Genomic insertion of mutated fragments in *S. cerevisiae***
832 To insert promoter mutations upstream of *FCY1*, competent yeast cells harboring a *natNT2*
833 deletion of the F3 or F4 region (strains SA0129 and SA0130) were transformed with the
834 corresponding PCR-amplified oPools. For each mutation category and each region, four
835 replicate transformations were performed from the corresponding four PCR reactions
836 described above – for a total of 24 transformations. The protocol described by Ryan *et al.*
837 (2016)[96] was followed (see *CRISPR-Cas9 yeast transformation*, above). After incubation,
838 G418-positive colonies from each agar plate were collected separately. Liquid YPD (5 ml) was
839 added to the plate, cells were resuspended by scraping with a glass rake and the suspension
840 was transferred to a 15 ml Falcon tube. From this suspension, glycerol stocks (687 µl cells
841 mixed with 313 µl sterile [80%] glycerol) were made for each transformation and stored at -
842 80°C. Two 500 µl aliquots from each tube were spun down and stored at -20°C after aspiration
843 of the supernatant. From these samples, mutant libraries were validated by PE150 sequencing
844 on an Illumina MiSeq instrument (Genomics Analysis Platform [PAG] of Institut de Biologie
845 Intégrative et des Systèmes, Université Laval, Québec). This approach was also employed to
846 insert the same set of promoter mutations upstream of the 42bp-mEGFP construct, using
847 strains SA0246 and SA0254. In this case, three replicate transformations were instead
848 performed per amplified oPool.
849
850 **Selection of coding sequence mutations**
851 Fifteen codon positions of the *FCY1* gene, for which all possible states had previously been
852 generated by DMS[36], were selected to obtain a diversity similar to that of the complete
853 mutational scanning of the F3-F4 region (15 positions x 64 codons = 960 mutants). Among
854 these positions, six were chosen for their wide range of variant effects and nine others were
855 selected randomly, to fully cover the previously reported range of mutational effects. The 15

856 corresponding pools of mutants were each grown for ~24 hours in 4 ml SC complete media
857 (30°C with shaking), from 25 µl of glycerol stock. Optical densities were measured and all
858 cultures were mixed in equal amounts to make four replicate 1 ml glycerol stocks (687 µl mixed
859 cultures and 313 µl sterile [80%] glycerol) of this pool of Fcy1p mutants, which were stored at
860 -80°C.
861
862 **Pooling of mutants**
863 The different sets of promoter mutations (substitutions, insertions and deletions, separately
864 for F3 and F4) were grown separately in 4 ml SC complete media, from 50-100 µl of the
865 corresponding glycerol stock. After ~16 hours of incubation at 30°C with shaking, $OD_{595}$ was
866 measured for all cultures. Subpools were then mixed to obtain equal proportions of all single
867 mutants, according to their $OD_{595}$ and how many unique genotypes they each contained.
868
869 For mutations in the *FCY1* background, the four replicate pools of coding sequence mutations
870 were also grown from 75 µl of glycerol stock. All subpools were then combined as described,
871 according to their replicate number (i.e. replicate 1 for F3 substitutions was mixed with
872 replicate 1 of all other subpools). Each subpool of promoter mutations was thus included in
873 only two final pools: one with added coding sequence mutations and the other without. For
874 mutations in the 42bp-mEGFP background, all subpools of promoter variants were combined
875 as described without the addition of other mutants, except that there were only three replicates
876 of each.
877
878 **Bulk competition experiment in 5-FC media**
879 Each mutant pool was grown in two replicates in 4 ml SC complete media (30°C, 200 rpm) for
880 ~20 hours, from 111 µl or 65 µl of the corresponding glycerol stock. These inoculum volumes
881 were chosen to have at least 2000x cells for each mutant, respectively for pools with and
882 without added coding sequence mutations. The competition experiment was initiated by
883 diluting each preculture at final $OD_{595}$ of 0.01 in 25 ml of SC complete media (with and without
884 5-FC [12 µM]) in 50 ml Falcon tubes. T0 samples were also prepared by centrifuging two
885 microtubes containing 5 $OD_{595}$ units for each preculture (850 g for 5 minutes; 4°C). After
886 aspiration of supernatant, cell pellets were stored at -20°C. Newly inoculated cultures were
887 incubated (30°C with shaking) in the dark until $OD_{595}$ reached ~1.0. At this first timepoint T1,
888 each culture was diluted in at final $OD_{595}$ of 0.01 in 25 ml of fresh media. Additional cell pellets
889 were prepared from the remaining cultures. The full volume was first centrifuged at 4°C (1000
890 g; 5 minutes). Cell pellets were resuspended in ~5 ml of supernatants and two samples of ~5
891 $OD_{595}$ units were prepared as previously. This process was repeated at timepoint T2 when the
892 new cultures reached $OD_{595}$ ~1.0 and final T3 samples were prepared when the newly
893 inoculated T2-T3 cultures reached the same $OD_{595}$. The timings of each timepoint and the
894 corresponding $OD_{595}$ values for all mutant pools are listed in **Supplementary Table 6**.
895
896 **Sort-seq experiment**
897 One final pool of F3-F4 mutants in the 42bp-mEGFP background was grown overnight from
898 100 µl glycerol stock in 5 ml of SC complete [pH = 6.0] media, at 30°C with shaking. After
899 measurement of its $OD_{595}$, the culture was diluted to 0.15 OD/ml in 20 ml of fresh SC complete
900 [pH = 6.0] and incubated for 5 hours at 30°C with shaking, to reach exponential phase (~0.5
901 OD/mL). From this, 4.5 ml were transferred to a 5 ml polystyrene round-bottom Falcon tube.

The remaining 15.5 ml were centrifuged to collect cells, so that genotype frequencies before sorting could also be measured by sequencing.

A FACSMelody cell sorter (BD Biosciences) was used to sort yeast cells based on their fluorescence intensity. Five bins were defined along the distribution of $log_{10}$ fluorescence intensities, numbered 0 to 4 from the lowest to the highest fluorescence levels (**Supplementary Methods**). More cells were collected from the most populated parts of the distribution (50 000 cells each from bins 2 and 3, versus 10 000 cells each from bins 0,1 and 4). Each bin was sorted twice, resulting in two technical replicates, in a 96 well plate. The resulting fractions were each used to inoculate 3 ml of SC complete [pH = 6.0] media in a 24 deep-well plate and grown for 24h at 30°C with shaking (400 rpm). Each culture was spun down at 3000 rpm (1000 g) for 5 min and all pellets were washed with sterile water and transferred to a 1.5 ml microtube. All microtubes were centrifuged at 15 000 rpm (21 000 g) for 1 min, supernatants were removed and pellets were frozen at -80°C. This process was repeated two times for the two other biological replicates, such that six replicate samples were obtained for each bin.

## DNA library preparation and sequencing

The same approach was used for all sequencing libraries, for both the bulk competition and sort-seq experiments. Genomic DNA was first extracted from each cell pellet using a standard phenol-chloroform extraction protocol[99], including RNAse treatment. For the resequencing of bulk competition samples in PE300, an additional RNAse treatment (10 minutes, 37°C) was performed on previously purified DNA samples, followed by precipitation with sodium acetate and cold ethanol. A first PCR was then performed using Q5 High-Fidelity DNA Polymerase (New England Biolabs) to amplify the genotyping region chosen for each type of samples, which included the F3-F4 promoter regions and flanking sequences of varying lengths. This PCR step added Illumina primer-binding sites at both ends, separated from the fragment of interest by small numbers of N bases (between 2 and 8; 10 total per PCR amplicon). For the initial (PE150) sequencing of bulk competition samples, primers CLOP311-C6 to CLOP314-H9 were used (as ordered in **Supplementary Table 2**). Two reactions were made from each DNA extraction from cultures with added coding sequence mutants. One was specific to the F3-F4 pool while the other targeted only the added *FCY1* variants. This was possible because the pool of coding sequence mutations was generated from a codon-optimized sequence, harboring many nucleotide changes from the WT [36]. For the PE300 resequencing of the same samples, only F3-F4 PCR were performed, using oligos CLOP328-A6 to CLOP328-H7. Finally, for the sequencing of sort-seq bins, also in PE300, oligos CLOP328-A6 to CLOP341-A10 were employed. In this case, 7 N bases were added per amplicon.

In all cases, amplicons from this first PCR step were purified with AMPure XP magnetic beads (Beckman Coulter Life Sciences) and diluted to 0.01 ng/µl. These dilutions were used as template for a second set of PCR reactions using Q5 polymerase, which added Nextera barcodes and Illumina adapters i5 and i7. A unique combination of i5 and i7 indexes was used for each DNA sample. The final PCR products were also purified with AMPure XP beads, before quantification using a NanoDrop spectrophotometer (Thermo Fisher Scientific). Amplicons from the same sequencing round (PE150 competition, PE300 competition or PE300 sort-seq) were mixed in equal proportions based on the NanoDrop quantification and the resulting pool was sent for sequencing. PE150 sequencing was performed on a NovaSeq

Illumina instrument (sequencing platform of Centre de recherche du CHU de Québec-Université Laval, Québec), while PE300 sequencing was performed on an AVITI instrument from Element Biosciences (Genomics Analysis Platform [PAG] of Institut de Biologie Intégrative et des Systèmes, Université Laval, Québec).

## Analysis of sequencing reads

Following each sequencing run, reads were received already demultiplexed, according to the sample id associated with each combination of i5 and i7 adaptors used. Read quality was first assessed using FastQC (v 0.12.1) and MultiQC (v 1.12)[100]. Paired-end reads were next merged using PANDAseq (v 2.11)[101], with the '-k' parameter set to 4. The N positions which had been added at both ends during the first PCR step of library construction were trimmed using command "fastx_filter" of VSEARCH (v 2.28.1)[102], according to a table listing the number of N added for each sample. The first and last 20 bp of the resulting sequences, which were the binding sites for the oligonucleotide primers used in the first PCR step, were also trimmed using the same command. Following these trimming steps, all identical sequences were aggregated with the "derep_fulllength" command of VSEARCH. Each unique sequence was aligned to the corresponding reference (depending on the type of sample and the length of the sequenced region) using the needle aligner from the EMBOSS suite (v 6.5.7)[103]. For promoter (F3-F4) libraries, the opening and extension of gaps was equally penalized (4,4), while penalties of 50 and 0.5 were respectively used for opening and extension for *FCY1* coding sequence libraries[36]. Custom Python functions were then used to call variants from each alignment. In addition to WT reads, only sequences harboring single-nucleotide mutations (F3-F4 libraries) or single-codon substitutions (*FCY1* libraries) were kept for downstream analysis. These variants were further filtered by length, to remove those that differed too much from the expected length of the PCR fragment. For bulk competition samples, read counts of each single mutant were converted to WT-relative frequencies. These read counts were instead used as is in the downstream analysis of sort-seq samples.

## Estimation of fitness effects

### Calculation of selection coefficients

For each bulk competition culture, time series of WT-relative genotype frequencies were reconstituted from variant frequencies obtained at the four timepoints (T0 to T3). The number of generations associated with each timepoint was obtained from the corresponding durations in hours, which varied between cultures, and the doubling time of the WT strain in the same conditions (SC media with or without 5-FC [12 µM]), as estimated from growth curve experiments. For each single-mutant genotype, the selection coefficient $s$ was obtained by fitting a linear model using the number of generations and the log-transformed WT-relative frequencies as dependent and independent variables, respectively. This was performed through ordinary least squares regression, using the "ols" implementation of the statsmodels (v 0.12.2)[104] Python module, with an intercept added to the model. Regressions were performed iteratively over all time intervals which included the T0 (T0-T1, T0-T2, T0-T3; with intermediate data points when applicable). Because selection coefficients were inferred separately within each culture replicate, as many replicate values as there were cultures were obtained for each of the intervals mentioned above.

To identify the selection coefficients which should be used in further analysis, two diagnostics were performed. First, the agreement between the initial (T0) log-scaled WT-relative

frequencies and the fitted intercept from each regression model was assessed. Second, the linearity of log-scaled frequencies through time, as expected for cultures growing exponentially, was validated graphically. This revealed that no interval was reliable for the initial 150 paired-end genotyping of promoter (F3-F4) libraries, while T0-T2 selection coefficients should be used for the 300 paired-end resequencing of the promoter fragments and the 150 paired-end sequence of *FCY1* coding sequence (see Supplementary Note). The chosen selection coefficients were then used to identify a T0 abundance threshold for variant filtering, such that inferred $s$ would not be correlated with initial read counts. This threshold was set at 85 reads, both for the promoter (300 paired-end) and coding sequence (150 paired-end) sequencing libraries. To ensure that low frequency but beneficial secondary mutations could be assessed, any variant which was below the threshold at T0 but over it at the end of the experiment was kept.

**Removal of outliers and aggregation of replicates**

In 5-FC samples, mutations sometimes appeared beneficial in only one pair of cultures (coming from the same transformation replicate), likely due to secondary resistance-conferring mutations (See Supplementary Note). Outlier removal was thus performed, separately for two types of libraries (promoter or coding sequence). The promoter (F3-F4) libraries were further separated depending on whether coding-sequence mutants had been added in the corresponding cultures. Within each group of samples, the median absolute deviation (MAD) of selection coefficients was first computed for each mutant. This was then used to compute robust z-scores for each replicate measurement within each genotype. The resulting distribution of robust z-scores calculated across all mutant genotypes was compared and its 95th percentile was defined as the threshold to identify outlier replicates. The filtering of outliers was however restricted to a subset of mutants which displayed a higher variance, to ensure that small absolute variations between replicates were not identified as outliers. This was assessed from each genotype's standard deviation, with the 95th percentile of the overall distribution used as threshold. For F3-F4 sequencing libraries obtained from cultures with added coding sequence mutations, the 85th percentile was instead used.

To obtain final estimates of the fitness effects of promoter mutations, only F3-F4 libraries without added coding sequence mutants were taken into account. Four of the eight replicate cultures, corresponding to two of the four transformation replicates, were additionally ignored. In these four samples, selection coefficients displayed a temporal shift towards negative values which appeared consistent with some undetected resistance-conferring mutations being genotyped as WT (see Supplementary Note). For each of the 1020 assayed promoter mutations, the corresponding fitness effect was estimated as the median of the selection coefficients observed across the four remaining replicates, which were considered unbiased.

The statistical significance of selection coefficients was assessed from the same four replicate measurements for each mutation, by comparing their mean to 0 using the SciPy (v 1.15.2)[105] implementation of the one-sample t-test, followed by Benjamini-Hochberg correction controlling the false discovery rate at 5%. For the coding sequence mutations added as controls, fitness effects were instead estimated as the median of the eight replicate measurements, without ignoring any of the corresponding samples. Alternatively, significant selection coefficients were also defined according to thresholds of minimal absolute deviations from 0, using the most extreme positive and negative replicates for each genotype. In this case, the number of fitness changes identified was compared with a null expectation derived

from the observed experimental noise. To this end, the complete dataset of final selection coefficients (from the four culture replicates mentioned above) was shuffled into 1020 random "genotypes". From each culture replicate, 1020 selection coefficients were first sampled with replacement. The resulting four sets of values were then combined randomly into the 1020 genotypes, such that each was associated with four replicate measurements. The number of random genotypes exceeding the chosen threshold of absolute deviation from 0 was then compiled. This was repeated 10 000 times.

## Comparison with published effects of amino acid substitutions in Fcy1p

The selection coefficients of added coding sequence mutations were first aggregated into grand medians, according to the corresponding amino acid substitutions. They were then compared with previously published variant effect scores obtained in the same conditions (12 µM 5-FC)[36]. The agreement between the two experiments was further assessed by classifying variants as resistant and susceptible in both cases. To this end, Gaussian mixture models with two components and a "tied" covariance matrix were fitted on each of the two datasets, using the scikit-learn (v 1.6.1)[106] implementation.

For the comparison of promoter and coding sequence mutations, the full dataset from[36] was used. All single-nucleotide substitutions in the reference sequence of the *FCY1* gene, obtained from the Saccharomyces Genome Database[98], were first performed computationally. The corresponding variant effects were retrieved from the Després *et al.* (2022) data[36], according to the resulting amino acid substitutions. Of 1431 possible single-nucleotide substitutions in *FCY1*, only 20 were not covered, mostly in the first and last codons. The Gaussian mixture model previously fitted on the full set of amino acid changes was then used to classify all single mutants as either resistant or susceptible. From this classification, the fraction of adaptive (resistance-conferring) mutations in the coding sequence was obtained.

## Calculation of sort-seq expression scores

Within each of the six replicate sort-seq experiments, all variants which reached a total abundance of at least 85 reads across the five sampled bins were kept for downstream analysis. Although this included a small number of secondary mutations (outside of the F3-F4 mutagenized region), any variant which occurred in the mEGFP sequence was filtered out. For each of the remaining genotypes $i$, which includes the WT, fluorescence intensity was quantified from a weighted average $B_i$ of bins where the corresponding reads were detected:

$$B_i = \frac{\sum_{j=0}^{4} j \frac{r_{i,j}}{r_{tot,j}} \frac{n_j}{n_{tot}}}{\sum_{j=0}^{4} \frac{r_{i,j}}{r_{tot,j}} \frac{n_j}{n_{tot}}}$$

In the previous formula, $j$ is the bin number, where 0 and 4 are associated with the lowest and highest fluorescence intensities, respectively. Variables $r_{i,j}$ and $r_{tot,j}$ are the read count for genotype $i$, as well as the total number of reads, in bin $j$. Finally, $n_j$ and $n_{tot}$ are respectively the number of cells collected from bin $j$ and the total amount of cells collected across the five bins. The $n_j/n_{tot}$ ratio was introduced because the number of yeast cells collected was not uniform across all bins.

Separately for each replicate experiment, the difference was computed between the $B_m$ weighted average of each mutant $m$ and the $B_{WT}$ weighted average obtained for the WT genotype:

$$\Delta_{Ref,m} = B_m - B_{WT}$$

For each mutant, up to six replicate $\Delta_{Ref}$ scores were obtained (one for each sort-seq experiment). The median of these values was used as an estimate of each mutation's effect on fluorescence intensity. Positive values denote an increase relative to the WT, while negative values instead indicate a decrease.

## Selection and construction of validation mutants

The sort-seq data was used to select 30 mutant genotypes for validation. These mutations were chosen to cover the whole range of scores, as well as all regions of the promoter where single-nucleotide changes appeared impactful. Substitutions were favored to ensure a high success rate to the downstream reconstruction of genotypes. To ensure that low-confidence mutations were not selected, a one-sample t-test (with Benjamini-Hochberg correction at FDR=5%) was first performed on the replicate sort-seq scores to identify $\Delta_{Ref}$ values which were significantly different from 0. This was also repeated with $\Delta_{mod}$ scores computed from $B_{mod}$ weighted averages obtained from reads of bin 1 to 4, excluding the 0th one displaying the lowest fluorescence intensities. Because the $\Delta_{Ref}$ scores appeared biased towards positive values compared with $\Delta_{mod}$, the latter were used to select significant mutations to be reconstructed, except when annotated *. This ensured a more stringent selection of genotypes displaying altered fluorescence intensity compared with the WT reference. Within each of the mutant groups described below, the specified number of sequences were chosen randomly, unless stated otherwise. Among mutations which significantly decreased $\Delta_{Mod}$ below zero, there were seven groups: 1) indels before the second methionine of *FCY1* (n=2); 2) indels after the second methionine of *FCY1* (n=2)*; 3) top 3 lowest scores between positions -50 and 0 of the promoter*; 4) substitutions between positions -133 and -127 (n=6); 5) substitutions between position -45 and -11 (n=2); 6) substitutions and insertions near the -75 position (one each) and 7) two chosen substitutions outside of regions with many significant effects. Among mutations which significantly increased $\Delta_{Mod}$ above zero, a similar approach was employed. The four categories were: 1) substitutions between position -125 and -118 (n=4); 2) substitutions between positions -112 to -109 (n=2); 3) substitutions between positions -63 to -57 (n=2) and 4) variants among the 25 highest scores (n=4).

The corresponding validation mutants were individually reconstructed using the CRISPR-Cas9 yeast transformation protocol described above. For each genotype, this was performed in two genetic backgrounds: fluorescent strain SA0247 (ΔF3-F4 with 42bp-mEGFP construct) and *FCY1* deletion (ΔF3-F4) mutant SA0159 (see **Supplementary Table 1**). A fusion PCR product harboring the single mutation of interest was used as donor DNA. This amplicon was generated by two consecutive rounds of PCR. In the first round, two reactions were performed with WT genomic DNA as template. The first one used a generic forward primer hybridizing upstream of F3 (CLOP326-A11) with a mutant-specific reverse primer harboring the mutation of interest (**Supplementary Table 2**). In the second reaction, a forward primer with the mutation of interest (**Supplementary Table 2**) was used alongside a generic reverse primer binding either in the mEGFP sequence (CLOP326-G10; for background SA0247) or in the *FCY1* coding sequence (CLOP326-E10; for background SA0159). The two mutant-specific mutagenesis primers are complementary to each other, such that there is homology between

1133 the two amplicons. The second PCR round used the two PCR products from the first round
1134 diluted 1/40 as template and the same two generic primers used in the first pair of PCR
1135 (CLOP326-A11 with either CLOP326-G10 or CLOP326-E10, depending on the mutagenized
1136 background), which allowed fusion of both PCR parts. This approach thus allows to amplify
1137 the full F3-F4 promoter region (with a short segment of *FCY1*) while introducing a single
1138 mutation within it and adding homology regions on both ends for subsequent genomic
1139 insertion. It was additionally used to perform deletion of short segments of the promoter (-133
1140 to -127 and -125 to -118), similarly in both genetic backgrounds. After transformation of each
1141 fusion PCR product, clones from each transformation were sent for Sanger sequencing to
1142 validate proper genomic integration of the mutation. All 66 resulting strains, including
1143 reconstructions of the WT promoter, are listed in **Supplementary Table 1**.
1144

## 1145 Expression measurements by flow cytometry

1146 Measurement of promoter activity using fluorescent strains was performed with a Guava
1147 EasyCyte HT cytometer (CytekBio). Each strain of interest was grown overnight in three
1148 replicates in SC complete media at 30°C with shaking, along with similar replicate cultures of
1149 a reference strain with the WT promoter (SA0247 or AKD1462) and of a non-fluorescent
1150 control (AKD1123 or AKD1429). The overnight cultures were diluted at 0.15 $OD_{595}$ in fresh
1151 SC-Trp (MSG) media and grown at 30°C with shaking until ~0.5 $OD_{595}$. Exponentially growing
1152 cells were then diluted to 0.05 $OD_{595}$ in fresh media and single-cell fluorescence intensity
1153 measurements were performed with the Guava EasyCyte HT system. For each replicate
1154 culture of each strain, 5000 events were acquired (488 nm excitation; 525 nm detection). The
1155 medians of the corresponding distributions of fluorescence intensities were used to estimate
1156 relative expression levels.
1157
1158 Within each cytometry experiment, events were first filtered out according to forward scatter
1159 and side scatter values, with the 99th percentile of each distribution used as thresholds. All
1160 fluorescence intensities were then normalized by the corresponding forward scatter
1161 measurement. From these normalized fluorescence intensities, a median was computed for
1162 each replicate culture assayed. These medians were then normalized by the grand median of
1163 measurements made for the reference strain, such that they were converted into WT-relative
1164 fluorescence intensities. The resulting values, and especially their medians, were used as
1165 estimates of relative expression levels. Accordingly, three replicate measurements of WT-
1166 relative fluorescence intensity were obtained for each tested strain, with a value of 1 being
1167 equal to the WT level.
1168

## 1169 Calibration of sort-seq scores and bootstrapping of relative expression 1170 levels

1171 WT-relative fluorescence intensities were first measured for all validation mutants
1172 reconstructed in the SA0247 (42bp-mEGFP) background, as described above. These
1173 measurements were then compared with the corresponding sort-seq expression scores and
1174 a LOWESS regression was fitted. This approach allowed to simultaneously validate the sort-
1175 seq experiments and convert the resulting scores into more interpretable WT-relative
1176 fluorescence intensities. The $\Delta_{Ref}$ scores were used, since some genotypes with very low
1177 fluorescence intensities were absent from the $\Delta_{mod}$ dataset. In addition, because
1178 fluorescence intensity measurements from reconstructed mutants were used to fit the
1179 relationship, any bias in $\Delta_{Ref}$ was unlikely to affect the downstream inference of relative

1180 expression levels. So that uncertainties could also be obtained for each of the >1000 mutant
1181 expression levels, both the LOWESS fitting and the conversion of sort-seq scores into relative
1182 fluorescence intensities were performed within a bootstrapping routine.
1183 At the start of each iteration, $\Delta_{Ref}$ scores were first resampled with replacement. For each
1184 genotype which had been included in the sort-seq analysis, as many values were sampled as
1185 there were replicate measurements among the six experiments. Per-genotype medians were
1186 then computed on the newly sampled data. For each reconstructed mutant for which
1187 fluorescence had been measured directly, three median WT-relative fluorescence intensities
1188 were sampled with replacement among the corresponding replicate measurements. Grand
1189 medians were computed from each trio of observations, which were combined with the newly
1190 recomputed median $\Delta_{Ref}$ scores of the corresponding validation genotypes to obtain 30 pairs.
1191 From these data points, LOWESS regression was performed with median $\Delta_{Ref}$ as
1192 independent variable, using the "nonparametric.lowess" implementation from statsmodels (v
1193 0.14.4)[104] with default parameters. This regression was then evaluated at each of the >1000
1194 median $\Delta_{Ref}$ values obtained from the first resampling steps. This generated an estimate of
1195 WT-relative fluorescence intensity for each of the genotypes which had been assayed in the
1196 sort-seq screen. The regression was also evaluated at 100 equally spaced values from the
1197 minimal to the maximal median $\Delta_{Ref}$ observed experimentally. This process was repeated
1198 5000 times. After all iterations had been completed, medians and corresponding 95%
1199 prediction intervals were computed from the distribution of WT-relative fluorescence intensities
1200 obtained for each mutant genotype. These medians were used as WT-relative expression
1201 levels associated with the corresponding F3-F4 mutations. The same calculations were
1202 performed for each of the 100 equally spaced values at which the LOWESS had been
1203 evaluated, thus allowing to plot the relationship between $\Delta_{Ref}$ and relative fluorescence
1204 intensity.
1205

## 1206 Experimental measurements of the expression-fitness function

### 1207 Fitting of dose-response curves

1208 The WT background AKD1123 was phenotyped in liquid media containing various
1209 concentrations of 5-FC and cytosine, according to the growth assays protocol described
1210 above. From two to three replicates were made for each concentration of 5-FC and cytosine.
1211 A five-parameter logistic model was then fitted, using the exponential growth rate
1212 measurements and the concentrations of 5-FC / cytosine as dependent and independent
1213 variables, respectively. The resulting curves were converted into relative inhibition or relative
1214 growth, using measured growth rates in absence of 5-FC or at the highest cytosine
1215 concentration as references.
1216

### 1217 Construction of strains with distinct *FCY1* expression levels

1218 Six yeast promoters covering a wide range of expression levels were used to construct two
1219 sets of strains, respectively from *FCY1* background AKD1123 and from fluorescent
1220 background SA0228. The six promoter cassettes, each including a G418 resistance marker,
1221 were PCR-amplified from the corresponding plasmids[95] (**Supplementary Table 3**) using
1222 oligonucleotides CLOP338-G6 and CLOP338-H6 (**Supplementary Table 2**). The two primers
1223 provided homology for genomic insertion immediately upstream of *FCY1* (or of its first 42 bp
1224 for the SA0228 background), between the gene and its native promoter. Yeast transformations
1225 were performed in the two genetic backgrounds as previously described, using each of the
1226 corresponding PCR products. Transformants were selected on YPD+HYG+G418 media.

1227 Correct integration of the promoter cassette was validated by PCR in four clones from each
1228 transformation, using oligonucleotides CLOP310-D1 and CLOP291-A3 (**Supplementary**
1229 **Table 2**). Two to three positive clones were obtained in most cases and validated by Sanger
1230 sequencing, such that biological replicates could be used in downstream assays for the
1231 majority of genotypes. All 25 corresponding yeast strains are listed in **Supplementary Table**
1232 **1**.
1233
1234 **Measurements of growth rates and fluorescence intensities**
1235 The set of *FCY1* strains (background AKD1123) was used to measure growth rates in liquid
1236 media containing different concentrations of 5-FC or cytosine, following the growth assays
1237 protocol described above. The set of fluorescent strains (background SA0228) was instead
1238 used in flow cytometry experiments to measure expression levels (see Expression
1239 measurements by flow cytometry). In both cases, all available biological replicates were used
1240 for each genotype. When less than three strains were available, three replicate cultures were
1241 nonetheless inoculated.
1242
1243 The growth assays in 5-FC media were performed in more than one experiment. To combine
1244 measurements obtained for concentrations of 12 µM and 3 µM (**Extended Data Fig. 9**), a
1245 normalization step was first performed.Growth rates from the first experiment were adjusted
1246 to have the same grand medians as those of the second one, by the addition of the difference
1247 between the two experiments' grand medians. This was performed separately for each
1248 concentration and allowed to combine the two sets of growth rates, in spite of potential
1249 systematic differences between them – for instance if the true concentration of 5-FC in the
1250 media varied. The cytometry measurements, which were done in parallel with the growth
1251 assays, were also performed in two separate experiments. In this case, potential systematic
1252 differences were controlled for by computing WT-relative fluorescence intensities within each
1253 experiment and only combining measurements after this step.
1254
1255 **Fitting of expression-fitness functions**
1256 Fluorescence measurements associated with each promoter were combined with the
1257 corresponding growth rates. Measurements made from the AKD1123 WT strain were however
1258 not used, because this strain lacks the G418 resistance marker included in promoter cassettes
1259 and is thus not directly comparable. An exponential function was fitted for each condition,
1260 using WT-relative fluorescence as the independent variable and growth rate as the dependent
1261 variable. This could model the sharp decline observed in 5-FC as well as the steep increase
1262 seen in cytosine conditions. The fitting of all expression-fitness curves was performed within
1263 a bootstrapping routine. For each promoter, two WT-relative fluorescence intensity
1264 measurements were first sampled with replacement from each cytometry experiment. Then,
1265 the four resulting values were resampled with replacement. Corresponding growth rates were
1266 sampled similarly. If a given condition had been tested in two experiments, two replicate
1267 growth rates were sampled with replacement from each experiment for each promoter, and
1268 the four measurements were afterwards resampled with replacement. This approach was
1269 employed to avoid favoring one experiment over the other, since the number of replicates
1270 sometimes varied between them. When only one experiment had been performed, replicate
1271 growth rates from this assay were instead resampled with replacement. Once relative
1272 fluorescence intensities and growth rates had been sampled, values obtained for the same
1273 promoter were paired randomly into data points. The exponential function was then fitted using
1274 the "optimize.curve_fit" implementation of the SciPy module (v 1.15.2)[105] module and

evaluated over 250 equally spaced values covering the full range of WT-relative fluorescence intensities. After 5000 iterations, medians and corresponding 95% prediction intervals were computed for each of these 250 fluorescence levels, thus generating the expression-fitness function. This was repeated for each of the 5-FC and cytosine concentrations tested.

**Inference of the expected distribution of effects on fitness for promoter mutations**

Changes in *FCY1* expression were assumed to have the same effect on fitness as variations in 5-FC concentration. The dose-response curve (**Extended Data Fig. 2**) was converted such that concentrations were expressed as relative changes from 12 µM (used in the bulk competition experiment). From this new curve, corresponding exponential growth rates were inferred for the 1019 relative expression estimates obtained from the sort-seq experiment. All growth rates were then converted into selection coefficients, as described above.

## Validation of *FCY1* promoter variants fitness effects

The previously described validation mutants reconstructed in the SA0159 *FCY1* background (**Supplementary Table 1**) were grown in SC complete (MSG) media with 12 µM 5-FC and without, according to the growth assays protocol described above. For all other mutants, growth rates measured in 12 µM 5-FC were converted into selection coefficients as described in the growth assays section, using growth rates measured in the same experiment for CRISPR reconstructions of the WT genotype in the SA0159 background (generated at the same time as the validation mutants). The expression-fitness function obtained in the same conditions and the bounds of its 95% prediction interval were also converted into selection coefficients using the same approach. In this case, the WT growth rate interpolated from the curve was instead used as comparison.

## Assessment of 5-FC resistance arising from mutant library construction

To test whether mutations conferring 5-FC resistance were introduced during mutant library construction, the process described in *Construction of mutant libraries* was repeated, but using WT sequences of the F3 and F4 regions. Briefly, the same two oligonucleotide pairs (CLOP299-C3/CLOP299-C4 and CLOP299-D3/CLOP299-D4) were first used to amplify F3 and F4 from genomic DNA of the AKD1123 strain, using KAPA HiFi HotStart DNA polymerase (Roche Molecular Systems). Competent cells from strains SA0129 and SA0130 (prepared as described by [96]) were then transformed with the F3 and F4 inserts, respectively. Two biological replicates of each transformation were made. This was performed following the CRISPR-Cas9 approach described above for the pools of single mutations. After 48 hours of incubation at 30°C, transformants from each Petri dish were collected in 5 ml YPD by scraping, as previously described. From each of the resulting cell suspension, cultures were started in 5 ml of SC complete [pH=6] + HYG, from 100 µl of cells.

After overnight incubation at 30°C with shaking, $OD_{595}$ was measured for each culture and dilutions at $OD_{595} = 1$ were made in 200 µl of sterile water. Additional dilutions were afterwards made for $OD_{595}$ values from 0.2 to 0.002. From each dilution, 150 µl were plated on SC complete (MSG) solid media with and without 5-FC [100 µg/ml]. Petri dishes were incubated at 30°C for 48 hours and colonies were counted. While colonies were too numerous to be counted on SC complete controls, some dilutions plated on 5-FC media resulted in countable colony numbers (between 20 and 340). For each plating (one per CRISPR-Cas9 transformation), colony counting was performed for two dilution levels, which acted as

technical replicates. Since the SA0130 background was initially resistant to 5-FC due to the insertion of a natNT2 in place of F4, all associated platings were replica plated on YPD+NAT media. Nourseothricin-resistant colonies were subtracted from the total number of 5-FC-resistant colonies. The frequency of 5-FC resistance was then estimated as follows, separately for each plating on media containing 5-FC:

$$F_{LOF} = \frac{n_{FC}}{OD_d \, V_{plate} \, c_{ml}}$$

In the equation above, $n_{FC}$ is the number of colonies on 5-FC media (after subtracting NAT resistant ones, when applicable), while $OD_d$ is the $OD_{595}$ of the plated dilution, $V_{plate}$ is the volume deposited on each plate (0.15 ml) and $c_{ml}$ is the number of yeast cells in 1 ml of media at $OD_{595} = 1$, for which a value of 10 million cells/ml was used. The resulting $F_{LOF}$ was considered as a putative frequency of *FCY1* LOF in the corresponding transformations. To validate whether that was the case, 16 colonies were selected for Sanger sequencing, using primer CLOP326-F10, which covered nearly 70% of the *FCY1* coding sequence **(Supplementary Table 2)**. All colony counts, resistance rates and relevant calculations are listed in **Supplementary Table 7**.

## Simulations with *invisible* resistance-conferring mutations

A simulation framework replicating the bulk competition experiment was designed. It involved a library of neutral variants within which a small number of invisible resistance-conferring mutations was introduced, thus mimicking secondary mutations occurring outside of the genotyping region in the experiment. A set of variants of interest (hereafter named genotype labels) was first generated by sampling 1000 neutral mutations from $s \sim \mathcal{N}(0, 0.004)$ four times. The standard deviation used was set according to what was observed in sequencing libraries from cultures without 5-FC. Four transformations were then obtained by replicate random samplings of 10 000 clones, among which 17% were defined as WT ($s = 0$) and the remaining were drawn from the set of genotype labels. Within each such transformation replicate, a small fraction of clones was defined as harboring an invisible resistance-conferring mutation (or resistance flag), which increased its $s$ (between 0.2 to 0.4, depending on simulations) without changing its genotype label. From each transformation, two replicate cultures were generated by randomly sampling two sets of 2.5 million cells, resulting in eight cultures, as in the bulk competition experiment (5-FC condition without added coding sequence variants). From each culture, 1 million of sequencing reads (genotype labels) were sampled randomly, to simulate sequencing of the initial T0 samples. Simulated cells in each culture were next aggregated according to genotype labels and presence/absence of a resistance flag, prior to calculation of WT-relative frequencies for each group (called true genotypes). Growth over the course of a bulk competition experiment was simulated by modeling exponential changes of WT-relative frequencies through time for each true genotype $i$, as follows:

$$F_{i,T+1} = F_{i,T} \, e^{s_i n_{gen}}$$

The WT-relative frequency $F$ of true genotype $i$ at timepoint $T+1$ is obtained from the corresponding WT-relative frequency at previous timepoint $T$ according to the genotype's true selection coefficient (increased by a resistance-conferring mutation when applicable) and the time interval $n_{gen}$ between the two timepoints, in WT generations. Three such timepoints, from T1 to T3, were simulated and their respective durations were set in accordance with the bulk competition experiment. At each timepoint, 1 million reads as well as a new initial population

of 2.5 million cells were sampled from each culture, as described above. Selection coefficients for all variants were then computed from time-series of simulated read counts, as described for experimental variant frequencies. This was performed from genotype labels only as well as with knowledge of true genotypes (resistance flags). Such simulations of one full experiment were repeated while varying both the initial frequency and the fitness effect of resistance-conferring mutations. For each combination, multiple replicate simulated experiments (each with eight simulated cultures) were performed.

## Data availability

All sequencing data from bulk competition and sort-seq experiments has been deposited on the NCBI SRA (https://www.ncbi.nlm.nih.gov/sra/PRJNA1321317). All other experimental data and files needed to replicate the analysis have been deposited on Zenodo: https://doi.org/10.5281/zenodo.17088129.

## Code availability

All analyses were performed using custom Python scripts and notebooks, which are available at: https://github.com/Landrylab/Aube_et_al_2025_FCY1promoter. A custom Python pipeline was deployed on a computing cluster (Institut de Biologie Intégrative et des Systèmes, Université Laval) to compute variant counts and selection coefficients from raw sequencing data. As described above, this used the following software: FastQC (v 0.12.1), MultiQC (v 1.12)[100], PANDAseq (v 2.11)[101], VSEARCH (v 2.28.1)[102] and EMBOSS suite (v 6.5.7)[103]. The versions of all Python modules used are included as requirements files, separately for the analysis pipeline and for the notebooks, which were executed locally.

## Acknowledgements

We thank Philippe Després, Isabelle Hatin, Olivier Namy and all Landry lab members, especially Soham Dibyachintan, David Jordan, Pascale Lemieux and Camille Bédard, for helpful discussions. We are grateful to Pavithra Venkataraman, Angel Cisneros, Soham Dibyachintan and Philippe Després, who provided comments on this manuscript. We additionally thank Angel Cisneros for helpful suggestions on the simulation framework. This work was supported by grants from the Natural Sciences and Engineering Research Council of Canada (NSERC RGPIN-2020-04844) and from the Human Frontier Science Program (HFSP RGP011/2025) to CRL. CRL holds the Canada Research Chair in Cellular Systems and Synthetic Biology. SA was supported by doctoral research fellowships from Natural Sciences and Engineering Research Council of Canada and Fonds de recherche du Québec - Nature et technologies. The F65V-34a-mEGFP plasmid used in this study was a kind gift from Dr Michael Springer.

## Author contributions

C.R.L., A.K.D and S.A. designed the study. S.A. and A.K.D. performed the experiments as well as the data analysis. S.A., A.K.D. and C.R.L. interpreted the results. S.A., A.K.D and C.R.L. wrote the manuscript.

1411

1412 ## References


1413 1. Keren, L. *et al.* Massively Parallel Interrogation of the Effects of Gene Expression Levels
1414 on Fitness. *Cell* **166**, 1282–1294.e18 (2016).
1415 2. Hill, M. S., Vande Zande, P. & Wittkopp, P. J. Molecular and evolutionary processes
1416 generating variation in gene expression. *Nat. Rev. Genet.* **22**, 203–215 (2021).
1417 3. Hodgins-Davis, A., Duveau, F., Walker, E. A. & Wittkopp, P. J. Empirical measures of
1418 mutational effects define neutral models of regulatory evolution in Saccharomyces
1419 cerevisiae. *Proceedings of the National Academy of Sciences* **116**, 21085–21093
1420 (2019).
1421 4. Vaishnav, E. D. *et al.* The evolution, evolvability and engineering of gene regulatory
1422 DNA. *Nature* **603**, 455–463 (2022).
1423 5. Tsuru, S., Hatanaka, N. & Furusawa, C. Promoters constrain evolution of expression
1424 levels of essential genes in Escherichia coli. *Mol. Biol. Evol.* **41**, msae185 (2024).
1425 6. Patwardhan, R. P. *et al.* High-resolution analysis of DNA regulatory elements by
1426 synthetic saturation mutagenesis. *Nat. Biotechnol.* **27**, 1173–1175 (2009).
1427 7. Patwardhan, R. P. *et al.* Massively parallel functional dissection of mammalian
1428 enhancers in vivo. *Nat. Biotechnol.* **30**, 265–270 (2012).
1429 8. Melnikov, A. *et al.* Systematic dissection and optimization of inducible enhancers in
1430 human cells using a massively parallel reporter assay. *Nat. Biotechnol.* **30**, 271–277
1431 (2012).
1432 9. Kircher, M. *et al.* Saturation mutagenesis of twenty disease-associated regulatory
1433 elements at single base-pair resolution. *Nat. Commun.* **10**, 3583 (2019).
1434 10. Duveau, F., Toubiana, W. & Wittkopp, P. J. Fitness effects of Cis-regulatory variants in
1435 the Saccharomyces cerevisiae TDH3 promoter. *Mol. Biol. Evol.* **34**, 2908–2912 (2017).
1436 11. Duveau, F. *et al.* Fitness effects of altering gene expression noise in Saccharomyces
1437 cerevisiae. *Elife* **7**, e37272 (2018).
1438 12. Siddiq, M. A., Duveau, F. & Wittkopp, P. J. Plasticity and environment-specific
1439 relationships between gene expression and fitness in Saccharomyces cerevisiae. *Nat.
1440 Ecol. Evol.* **8**, 2184–2194 (2024).
1441 13. Rich, M. S. *et al.* Comprehensive Analysis of the SUL1 Promoter of Saccharomyces
1442 cerevisiae. *Genetics* **203**, 191–202 (2016).
1443 14. Sanchez, M. R. *et al.* Differential paralog divergence modulates genome evolution
1444 across yeast species. *PLoS Genet.* **13**, e1006585 (2017).
1445 15. McManus, K. F. *et al.* Population genetic analysis of the DARC locus (Duffy) reveals
1446 adaptation from standing variation associated with malaria resistance in humans. *PLoS
1447 Genet.* **13**, e1006560 (2017).
1448 16. Tournamille, C., Colin, Y., Cartron, J. P. & Le Van Kim, C. Disruption of a GATA motif in
1449 the Duffy gene promoter abolishes erythroid gene expression in Duffy-negative
1450 individuals. *Nat. Genet.* **10**, 224–228 (1995).
1451 17. Breeyear, J. H. *et al.* Adaptive selection at G6PD and disparities in diabetes
1452 complications. *Nat. Med.* **30**, 2480–2488 (2024).
1453 18. Chan, Y. F. *et al.* Adaptive evolution of pelvic reduction in sticklebacks by recurrent
1454 deletion of a Pitx1 enhancer. *Science* **327**, 302–305 (2010).
1455 19. Bédard, C. *et al.* FungAMR: a comprehensive database for investigating fungal
1456 mutations associated with antimicrobial resistance. *Nat. Microbiol.* (2025)

1457 doi:10.1038/s41564-025-02084-7.
1458 20. Guerrero-Preston, R. *et al.* Key tumor suppressor genes inactivated by 'greater
1459 promoter' methylation and somatic mutations in head and neck cancer. *Epigenetics* **9**,
1460 1031–1046 (2014).
1461 21. Behe, M. J. Experimental evolution, loss-of-function mutations, and 'the first rule of
1462 adaptive evolution'. *Q. Rev. Biol.* **85**, 419–445 (2010).
1463 22. Gerstein, A. C., Lo, D. S. & Otto, S. P. Parallel Genetic Changes and Nonparallel Gene–
1464 Environment Interactions Characterize the Evolution of Drug Resistance in Yeast.
1465 *Genetics* **192**, 241–252 (2012).
1466 23. Kvitek, D. J. & Sherlock, G. Whole genome, whole population sequencing reveals that
1467 loss of signaling networks is the major adaptive strategy in a constant environment.
1468 *PLoS Genet.* **9**, e1003972 (2013).
1469 24. Lang, G. I. & Desai, M. M. The spectrum of adaptive mutations in experimental
1470 evolution. *Genomics* **104**, 412–416 (2014).
1471 25. Lind, P. A., Libby, E., Herzog, J. & Rainey, P. B. Predicting mutational routes to new
1472 adaptive phenotypes. *Elife* **8**, e38822 (2019).
1473 26. Murray, A. W. Can gene-inactivating mutations lead to evolutionary novelty? *Curr. Biol.*
1474 **30**, R465–R471 (2020).
1475 27. Durand, R., Jalbert-Ross, J., Fijarczyk, A., Dubé, A. K. & Landry, C. R. Cross-feeding
1476 affects the target of resistance evolution to an antifungal drug. *PLoS Genet.* **19**,
1477 e1011002 (2023).
1478 28. Chen, P. & Zhang, J. The loci of environmental adaptation in a model eukaryote. *Nat.*
1479 *Commun.* **15**, 5672 (2024).
1480 29. Ascencio, D. *et al.* Expression attenuation as a mechanism of robustness against gene
1481 duplication. *Proc. Natl. Acad. Sci. U. S. A.* **118**, e2014345118 (2021).
1482 30. Cools, H. J., Hawkins, N. J. & Fraaije, B. A. Constraints on the evolution of azole
1483 resistance in plant pathogenic fungi. *Plant Pathol.* **62**, 36–42 (2013).
1484 31. Todd, R. T. & Selmecki, A. Expandable and reversible copy number amplification drives
1485 rapid adaptation to antifungal drugs. *Elife* **9**, e58349 (2020).
1486 32. Gresham, D. *et al.* The repertoire and dynamics of evolutionary adaptations to
1487 controlled nutrient-limited environments in yeast. *PLoS Genet.* **4**, e1000303 (2008).
1488 33. Payen, C. *et al.* The dynamics of diverse segmental amplifications in populations of
1489 Saccharomyces cerevisiae adapting to strong selection. *G3 (Bethesda)* **4**, 399–409
1490 (2014).
1491 34. Jay, A., Jordan, D. F., Gerstein, A. & Landry, C. R. The role of gene copy number
1492 variation in antimicrobial resistance in human fungal pathogens. *NPJ Antimicrob Resist*
1493 **3**, 1 (2025).
1494 35. Vermes, A., Guchelaar, H. J. & Dankert, J. Flucytosine: a review of its pharmacology,
1495 clinical indications, pharmacokinetics, toxicity and drug interactions. *J. Antimicrob.*
1496 *Chemother.* **46**, 171–179 (2000).
1497 36. Després, P. C. *et al.* Asymmetrical dose responses shape the evolutionary trade-off
1498 between antifungal resistance and nutrient use. *Nat. Ecol. Evol.* **6**, 1501–1515 (2022).
1499 37. Lin, Z., Wu, W.-S., Liang, H., Woo, Y. & Li, W.-H. The spatial distribution of cis
1500 regulatory elements in yeast promoters and its implications for transcriptional regulation.
1501 *BMC Genomics* **11**, 581 (2010).
1502 38. Mahendrawada, L., Warfield, L., Donczew, R. & Hahn, S. Low overlap of transcription
1503 factor DNA binding and regulatory targets. *Nature* **642**, 796–804 (2025).
1504 39. Lemieux, P., Bradley, D., Dubé, A. K., Dionne, U. & Landry, C. R. Dissection of the role

1505 of a Src homology 3 domain in the evolution of binding preference of paralogous
1506 proteins. *Genetics* **226**, iyad175 (2024).
1507 40. Dionne, U. *et al.* Protein context shapes the specificity of SH3 domain-mediated
1508 interactions in vivo. *Nat. Commun.* **12**, 1597 (2021).
1509 41. Matuszewski, S., Hildebrandt, M. E., Ghenu, A.-H., Jensen, J. D. & Bank, C. A statistical
1510 guide to the design of deep mutational scanning experiments. *Genetics* **204**, 77–87
1511 (2016).
1512 42. de Boer, C. G. *et al.* Deciphering eukaryotic gene-regulatory logic with 100 million
1513 random promoters. *Nat. Biotechnol.* **38**, 56–65 (2020).
1514 43. Peterman, N. & Levine, E. Sort-seq under the hood: implications of design choices on
1515 large-scale characterization of sequence-function relations. *BMC Genomics* **17**, 206
1516 (2016).
1517 44. Eisenberg, A. R. *et al.* Translation initiation site profiling reveals widespread synthesis of
1518 non-AUG-initiated protein isoforms in yeast. *Cell Syst.* **11**, 145–160.e5 (2020).
1519 45. Huang, Q., Szklarczyk, D., Wang, M., Simonovic, M. & von Mering, C. PaxDb 5.0:
1520 Curated protein quantification data suggests adaptive proteome changes in yeasts. *Mol.*
1521 *Cell. Proteomics* **22**, 100640 (2023).
1522 46. de Boer, C. G. & Hughes, T. R. YeTFaSCo: a database of evaluated yeast transcription
1523 factor sequence specificities. *Nucleic Acids Res.* **40**, D169–79 (2012).
1524 47. Rhee, H. S. & Pugh, B. F. Genome-wide structure and organization of eukaryotic pre-
1525 initiation complexes. *Nature* **483**, 295–301 (2012).
1526 48. McMillan, J., Lu, Z., Rodriguez, J. S., Ahn, T.-H. & Lin, Z. YeasTSS: an integrative web
1527 database of yeast transcription start sites. *Database (Oxford)* **2019**, baz048 (2019).
1528 49. Metzger, B. P. H. *et al.* Contrasting Frequencies and Effects of cis- and trans-
1529 Regulatory Mutations Affecting Gene Expression. *Mol. Biol. Evol.* **33**, 1131–1146
1530 (2016).
1531 50. Erb, I. & van Nimwegen, E. Transcription factor binding site positioning in yeast:
1532 proximal promoter motifs characterize TATA-less promoters. *PLoS One* **6**, e24279
1533 (2011).
1534 51. Park, D., Morris, A. R., Battenhouse, A. & Iyer, V. R. Simultaneous mapping of transcript
1535 ends at single-nucleotide resolution and identification of widespread promoter-
1536 associated non-coding RNA governed by TATA elements. *Nucleic Acids Res.* **42**, 3736–
1537 3749 (2014).
1538 52. Pelechano, V., Wei, W. & Steinmetz, L. M. Extensive transcriptional heterogeneity
1539 revealed by isoform profiling. *Nature* **497**, 127–131 (2013).
1540 53. Struhl, K. Naturally occurring poly(dA-dT) sequences are upstream promoter elements
1541 for constitutive transcription in yeast. *Proc. Natl. Acad. Sci. U. S. A.* **82**, 8419–8423
1542 (1985).
1543 54. de Boer, C. G. & Hughes, T. R. Poly-dA:dT tracts form an in vivo nucleosomal turnstile.
1544 *PLoS One* **9**, e110479 (2014).
1545 55. Ichikawa, Y. *et al.* Sequence-directed nucleosome-depletion is sufficient to activate
1546 transcription from a yeast core promoter in vivo. *Biochem. Biophys. Res. Commun.* **476**,
1547 57–62 (2016).
1548 56. Jansen, A., van der Zande, E., Meert, W., Fink, G. R. & Verstrepen, K. J. Distal
1549 chromatin structure influences local nucleosome positions and gene expression. *Nucleic*
1550 *Acids Res.* **40**, 3870–3885 (2012).
1551 57. Delma, F. Z. *et al.* Genetic mutations in Cryptococcus neoformans pyrimidine salvage
1552 pathway enzymes contribute to reduced susceptibility against 5-fluorocytosine. *NPJ*

1553 *Antimicrob. Resist.* **2**, 24 (2024).
1554 58. Kruglyak, L. *et al.* Insufficient evidence for non-neutrality of synonymous mutations.
1555 *Nature* **616**, E8–E9 (2023).
1556 59. Wyman, S. K. *et al.* Synthesis errors in oligonucleotides are propagated into the
1557 genome by homology-directed repair. *bioRxiv* 2025.07.08.663753 (2025)
1558 doi:10.1101/2025.07.08.663753.
1559 60. Metzger, B. P. H., Yuan, D. C., Gruber, J. D., Duveau, F. & Wittkopp, P. J. Selection on
1560 noise constrains variation in a eukaryotic promoter. *Nature* **521**, 344–347 (2015).
1561 61. Payen, C. *et al.* High-throughput identification of adaptive mutations in experimentally
1562 evolved yeast populations. *PLoS Genet.* **12**, e1006339 (2016).
1563 62. Ho, B., Baryshnikova, A. & Brown, G. W. Unification of Protein Abundance Datasets
1564 Yields a Quantitative Saccharomyces cerevisiae Proteome. *Cell Syst* **6**, 192–205.e3
1565 (2018).
1566 63. Hartl, D. L., Dykhuizen, D. E. & Dean, A. M. Limits of adaptation: the evolution of
1567 selective neutrality. *Genetics* **111**, 655–674 (1985).
1568 64. Zhu, Y. O., Siegal, M. L., Hall, D. W. & Petrov, D. A. Precise estimates of mutation rate
1569 and spectrum in yeast. *Proc. Natl. Acad. Sci. U. S. A.* **111**, E2310–8 (2014).
1570 65. Basehoar, A. D., Zanton, S. J. & Pugh, B. F. Identification and distinct regulation of
1571 yeast TATA box-containing genes. *Cell* **116**, 699–709 (2004).
1572 66. Rossi, M. J. *et al.* A high-resolution protein architecture of the budding yeast genome.
1573 *Nature* **592**, 309–314 (2021).
1574 67. Jin, Z. *et al.* Unraveling the regulatory dynamics of bidirectional promoters for
1575 modulating gene co-expression and metabolic flux in Saccharomyces cerevisiae.
1576 *Nucleic Acids Res.* **53**, gkaf511 (2025).
1577 68. Kemble, H., Nghe, P. & Tenaillon, O. Recent insights into the genotype-phenotype
1578 relationship from massively parallel genetic assays. *Evol. Appl.* **12**, 1721–1742 (2019).
1579 69. Kacser, H. & Burns, J. A. The molecular basis of dominance. *Genetics* **97**, 639–666
1580 (1981).
1581 70. Dykhuizen, D. E., Dean, A. M. & Hartl, D. L. Metabolic flux and fitness. *Genetics* **115**,
1582 25–31 (1987).
1583 71. Rest, J. S. *et al.* Nonlinear fitness consequences of variation in expression level of a
1584 eukaryotic gene. *Mol. Biol. Evol.* **30**, 448–456 (2013).
1585 72. Jiang, L., Mishra, P., Hietpas, R. T., Zeldovich, K. B. & Bolon, D. N. A. Latent effects of
1586 Hsp90 mutants revealed at reduced expression levels. *PLoS Genet.* **9**, e1003600
1587 (2013).
1588 73. Hackett, S. R. *et al.* Systems-level analysis of mechanisms regulating yeast metabolic
1589 flux. *Science* **354**, aaf2786–aaf2786 (2016).
1590 74. Zhang, C. *et al.* Yeast9: a consensus genome-scale metabolic model for S. cerevisiae
1591 curated by the community. *Mol. Syst. Biol.* **20**, 1134–1150 (2024).
1592 75. Li, X., Walhout, A. J. M. & Yilmaz, L. S. Enhanced flux potential analysis links changes
1593 in enzyme expression to metabolic flux. *Mol. Syst. Biol.* **21**, 413–445 (2025).
1594 76. Vanella, R. *et al.* Understanding activity-stability tradeoffs in biocatalysts by enzyme
1595 proximity sequencing. *Nat. Commun.* **15**, 1807 (2024).
1596 77. Amorosi, C. J. *et al.* Massively parallel characterization of CYP2C9 variant enzyme
1597 activity and abundance. *Am. J. Hum. Genet.* **108**, 1735–1751 (2021).
1598 78. Prywes, N. *et al.* A map of the rubisco biochemical landscape. *Nature* **638**, 823–828
1599 (2025).
1600 79. Grønbæk-Thygesen, M. *et al.* Deep mutational scanning reveals a correlation between

1601 degradation and toxicity of thousands of aspartoacylase variants. *Nat. Commun.* **15**,
1602 4026 (2024).
1603 80. Beltran, A., Jiang, X. 'er, Shen, Y. & Lehner, B. Site-saturation mutagenesis of 500
1604 human protein domains. *Nature* **637**, 885–894 (2025).
1605 81. Bédard, C. *et al.* Most azole resistance mutations in the Candida albicans drug target
1606 confer cross-resistance without intrinsic fitness cost. *Nat. Microbiol.* **9**, 3025–3040
1607 (2024).
1608 82. Tabet, D. R. *et al.* The functional landscape of coding variation in the familial
1609 hypercholesterolemia gene LDLR. *Science* eady7186 (2025)
1610 doi:10.1126/science.ady7186.
1611 83. Cisneros, A. F. *et al.* Epistasis between promoter activity and coding mutations shapes
1612 gene evolvability. *Sci. Adv.* **9**, eadd9109 (2023).
1613 84. Risch, T. *et al.* YgiV promoter mutations cause resistance to cystobactamids and
1614 reduced virulence factor expression in Escherichia coli. *NPJ Antimicrob. Resist.* **2**, 33
1615 (2024).
1616 85. Händel, N., Schuurmans, J. M., Feng, Y., Brul, S. & ter Kuile, B. H. Interaction between
1617 mutations and regulation of gene expression during development of de novo antibiotic
1618 resistance. *Antimicrob. Agents Chemother.* **58**, 4371–4379 (2014).
1619 86. Siu, L. K., Ho, P. L., Yuen, K. Y., Wong, S. S. & Chau, P. Y. Transferable
1620 hyperproduction of TEM-1 beta-lactamase in Shigella flexneri due to a point mutation in
1621 the pribnow box. *Antimicrob. Agents Chemother.* **41**, 468–470 (1997).
1622 87. Chang, J. *et al.* The molecular mechanism of a cis-regulatory adaptation in yeast. *PLoS*
1623 *Genet.* **9**, e1003813 (2013).
1624 88. Sharon, E. *et al.* Functional genetic variants revealed by massively parallel precise
1625 genome editing. *Cell* **175**, 544–557.e16 (2018).
1626 89. Hoekstra, H. E. & Coyne, J. A. The locus of evolution: evo devo and the genetics of
1627 adaptation: The locus of evolution. *Evolution* **61**, 995–1016 (2007).
1628 90. Brown, K. M., Depristo, M. A., Weinreich, D. M. & Hartl, D. L. Temporal constraints on
1629 the incorporation of regulatory mutants in evolutionary pathways. *Mol Biol Evol* **26**,
1630 2455–2462 (2009).
1631 91. Groover, E. D. *et al.* Mapping cis-regulatory mutations at scale in sorghum enables
1632 modulation of gene expression. *Nat. Biotechnol.* 1–11 (2026) doi:10.1038/s41587-026-
1633 03046-y.
1634 92. Milind, N. *et al.* Buffering and non-monotonic behavior of gene dosage response curves
1635 for human complex traits. *medRxiv* 2024.11.11.24317065 (2025)
1636 doi:10.1101/2024.11.11.24317065.
1637 93. Brachmann, C. B. *et al.* Designer deletion strains derived from Saccharomyces
1638 cerevisiae S288C: a useful set of strains and plasmids for PCR-mediated gene
1639 disruption and other applications. *Yeast* **14**, 115–132 (1998).
1640 94. Gietz, R. D. & Schiestl, R. H. High-efficiency yeast transformation using the LiAc/SS
1641 carrier DNA/PEG method. *Nat. Protoc.* **2**, 31–34 (2007).
1642 95. Janke, C. *et al.* A versatile toolbox for PCR-based tagging of yeast genes: new
1643 fluorescent proteins, more markers and promoter substitution cassettes. *Yeast* **21**, 947–
1644 962 (2004).
1645 96. Ryan, O. W., Poddar, S. & Cate, J. H. D. CRISPR-Cas9 Genome Engineering in
1646 Saccharomyces cerevisiae Cells. *Cold Spring Harb. Protoc.* **2016**, db.prot086827
1647 (2016).
1648 97. Chevin, L.-M. On measuring selection in experimental evolution. *Biol. Lett.* **7**, 210–213

(2011).
98. Engel, S. R. *et al.* Saccharomyces Genome Database: advances in genome annotation, expanded biochemical pathways, and other key enhancements. *Genetics* **229**, iyae185 (2025).
99. Amberg, D. C., Burke, D. J. & Strathern, J. N. *Methods in Yeast Genetics 2005: A Cold Spring Harbor Laboratory Course Manual*. (Cold Spring Harbor Laboratory Press, New York, NY, 2005).
100. Ewels, P., Magnusson, M., Lundin, S. & Käller, M. MultiQC: summarize analysis results for multiple tools and samples in a single report. *Bioinformatics* **32**, 3047–3048 (2016).
101. Masella, A. P., Bartram, A. K., Truszkowski, J. M., Brown, D. G. & Neufeld, J. D. PANDAseq: paired-end assembler for illumina sequences. *BMC Bioinformatics* **13**, 31 (2012).
102. Rognes, T., Flouri, T., Nichols, B., Quince, C. & Mahé, F. VSEARCH: a versatile open source tool for metagenomics. *PeerJ* **4**, e2584 (2016).
103. Rice, P., Longden, I. & Bleasby, A. EMBOSS: The European molecular biology open software suite. *Trends Genet.* **16**, 276–277 (2000).
104. Seabold, S. & Perktold, J. statsmodels: Econometric and statistical modeling with python. in *9th Python in Science Conference* (2010).
105. Virtanen, P. *et al.* SciPy 1.0: fundamental algorithms for scientific computing in Python. *Nat. Methods* **17**, 261–272 (2020).
106. Pedregosa, F. *et al.* Scikit-learn: Machine Learning in Python. *Journal of Machine Learning Research* **12**, 2825–2830 (2011).
107. Chereji, R. V., Ramachandran, S., Bryson, T. D. & Henikoff, S. Precise genome-wide mapping of single nucleosomes and linkers in vivo. *Genome Biol.* **19**, 19 (2018).

1684 **Extended Data Figures:**

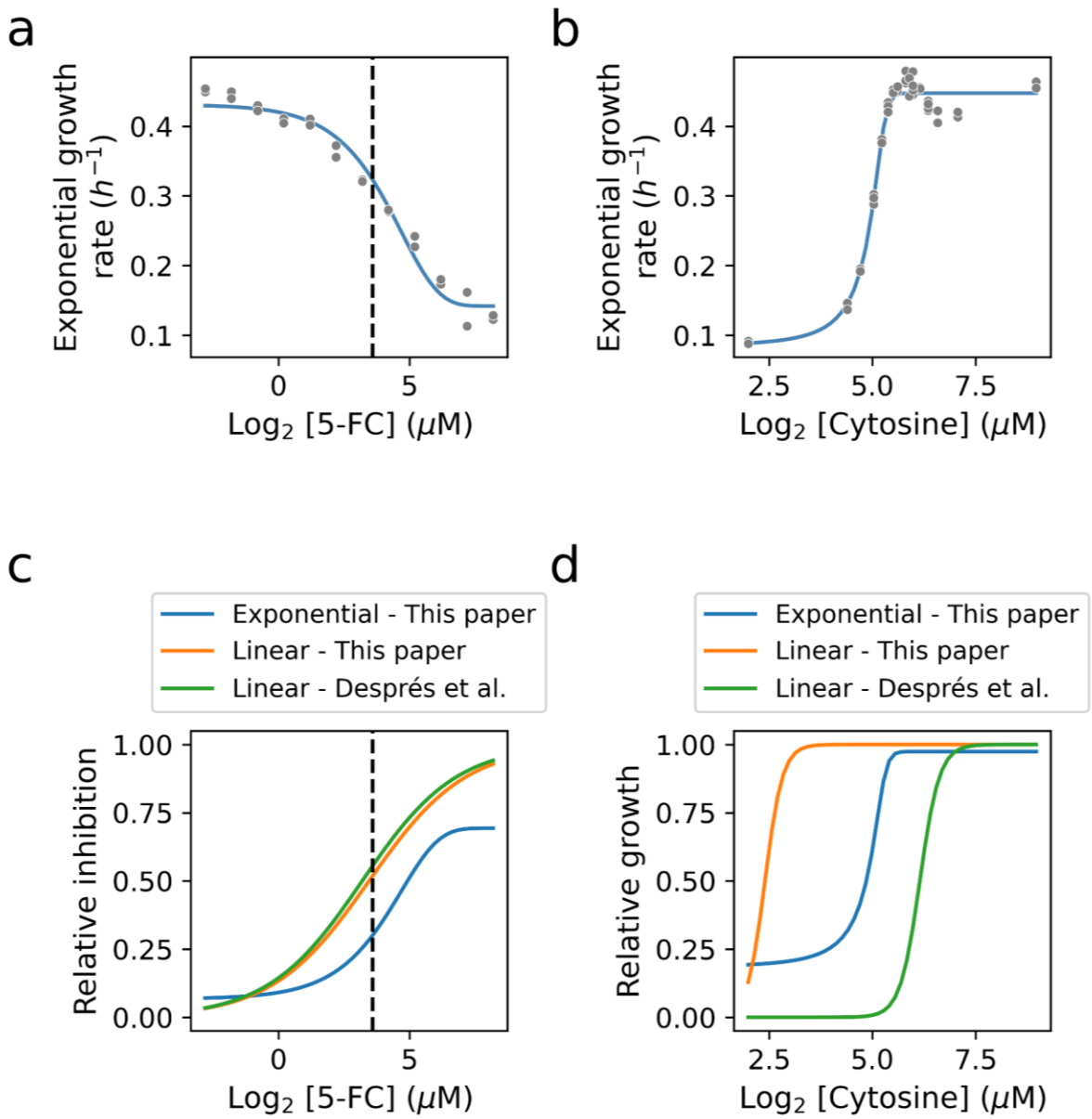


1685
1686 **Extended Data Fig. 1: The growth rate of wild-type yeast varies sharply across a range of 5-FC**
1687 **and cytosine concentrations. a,** Exponential growth rates for the wild-type reference strain AKD1123
1688 across 5-FC concentrations. Two replicate cultures were assayed for each tested concentration (dots).
1689 The line displays a fitted five-parameter logistic function (Methods), while the vertical dashed line
1690 identifies the 12 μM concentration used in the bulk competition experiment. b, Same as panel a, but for
1691 a range of cytosine concentrations in media lacking uracil. c, The dose-response curve obtained for 5-
1692 FC is consistent with a previously published relationship. The curve from a is shown after conversion
1693 into relative inhibition levels, using growth rates measured in absence of 5-FC within the same
1694 experiment as comparison (0 relative inhibition). This curve, labeled "Exponential - This paper", was
1695 used in downstream analyses to obtain the relative inhibition level associated with a given 5-FC
1696 concentration. When the same growth curve data is used to compute maximum linear growth rates
1697 (rather than exponential growth rates) and then fit a dose-response curve as in Després et al.[36], the
1698 published relationship is replicated. d, Same as panel c, but using the cytosine growth data shown in
1699 panel b. Here, the published relationship cannot be replicated by using the same analysis approach.

The curve, labeled “Exponential - This paper”, was nonetheless used in downstream analyses to obtain relative growth levels.

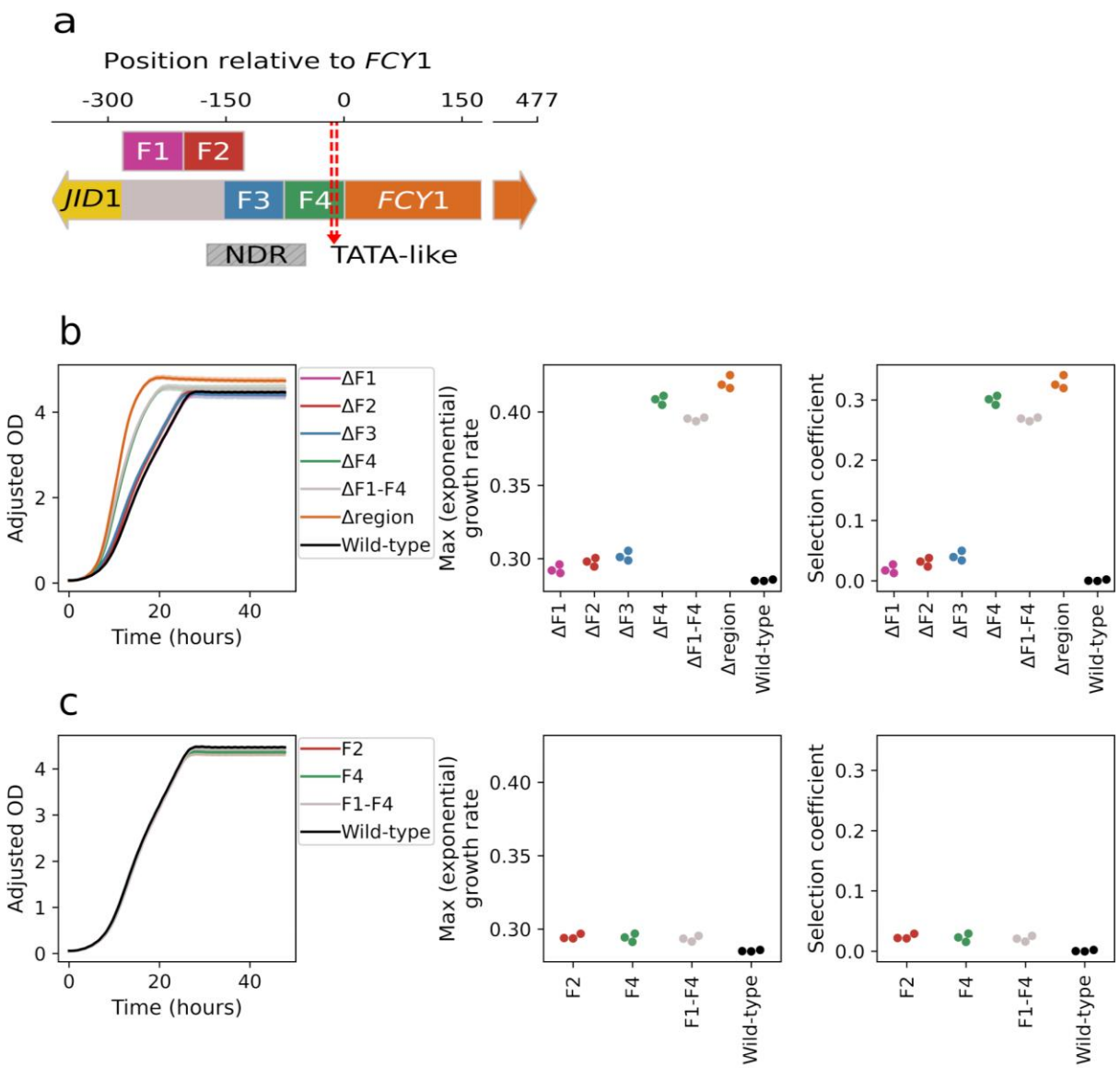


**Extended Data Fig. 2**: **The deletion of the F4 promoter fragment is clearly adaptive in 5-FC conditions. a,** Schematics of the four 77 bp fragments into which the intergenic region between *JID1* (YPR061C) and *FCY1* (YPR062W) was divided. There is a 26 bp overlap between F2 and F3. The nucleosome-depleted region (NDR) of the corresponding bidirectional promoter[67,107] as well as the TATA-like element, involved in transcription initiation at *FCY1*[47,48], are shown. **b,** Fitness of deletion mutants in [12 μM] 5-FC. The ΔF1-F4 mutant refers to deletion of the complete intergenic region, while Δregion instead represents the simultaneous deletion of the intergenic region and the *FCY1* gene. Exponential growth rates and the corresponding selection coefficients (*Methods*) show that F4 is the only promoter fragment for which deletion confers a clear growth advantage (and thus 5-FC resistance). **c,** Fitness of reconstructed WT strains in [12 μM] 5-FC. Here, F2, F4 and F1-F4 refer to CRISPR reconstruction of the WT intergenic region from the corresponding deletion mutant (*Methods*). In all three cases, the WT 5-FC sensitivity is recovered. All growth measurements were made from three replicate cultures of each strain.

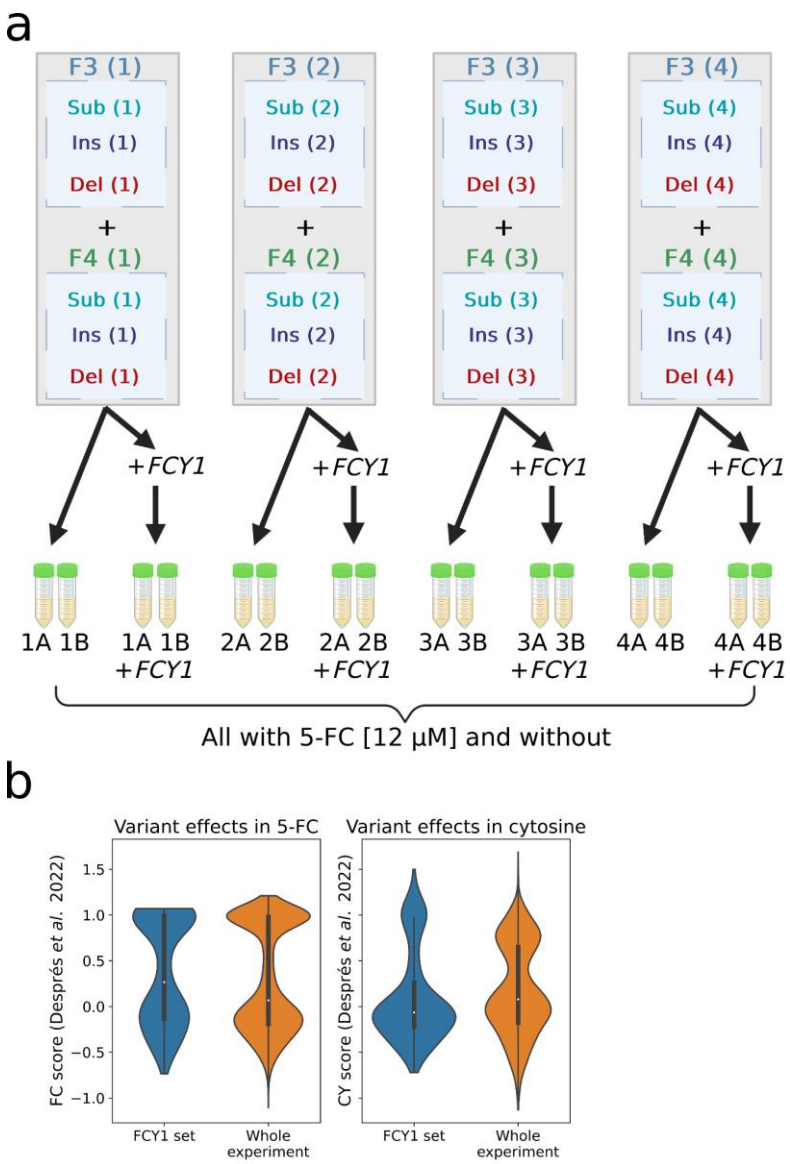


**Extended Data Fig. 3: Complete overview of the bulk competition experiment. a,** Full experimental design showing all 32 cultures and their relationships as transformation and/or culture replicates. Each pool of substitutions (Sub), insertions (Ins) or deletions (Del) was constructed four times and corresponding replicates were mixed to obtain each of the four *transformation replicates* (grey rectangles). Each transformation replicate was used to inoculate two culture replicates, with or without the addition of a set of previously characterized coding sequence mutations (*FCY1*; n=960)[36]. Created in BioRender. Aubé, S. (2025) https://BioRender.com/acpk3ks. **b,** The selected coding sequence variants cover the full range of variant effects reported in[36], both in 5-FC and cytosine (without uracil) conditions, where Fcy1 activity is respectively toxic and essential.

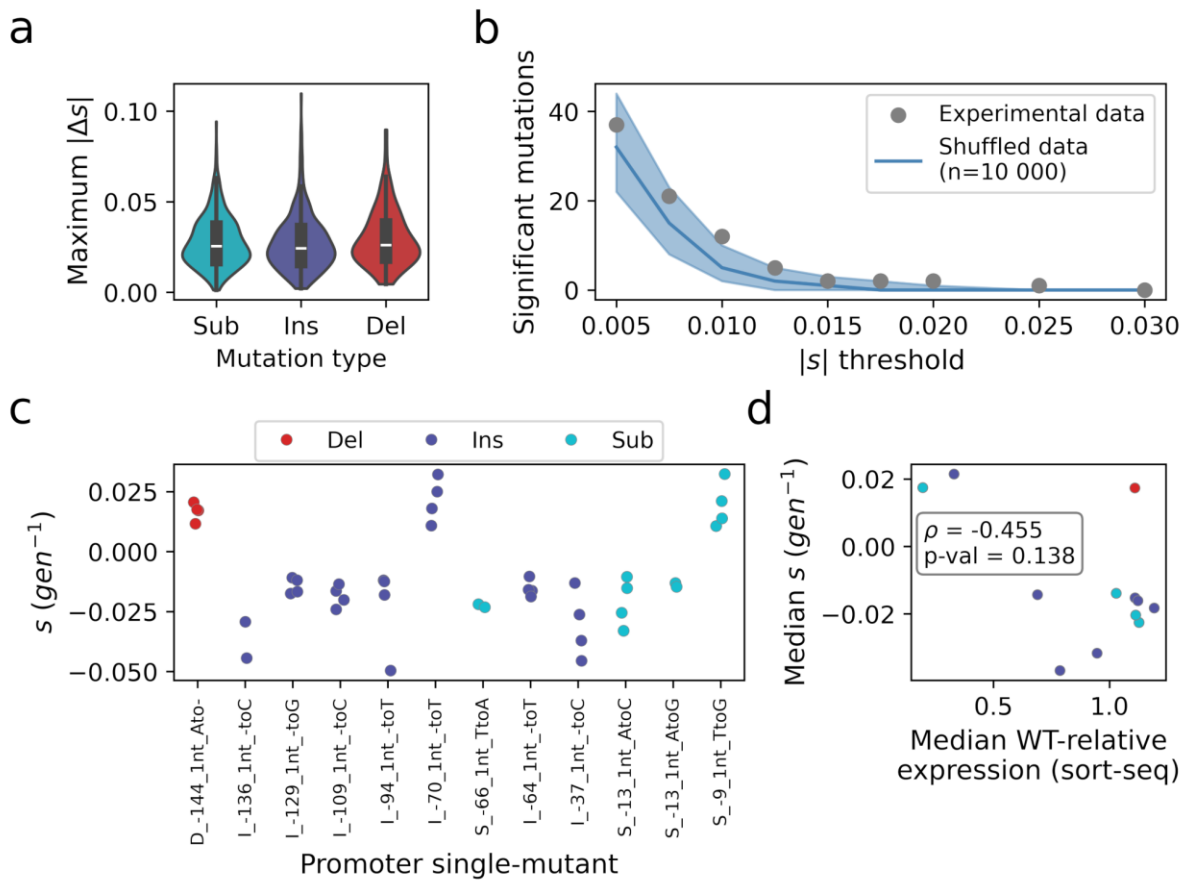


**Extended Data Fig. 4: The number and magnitude of small fitness effects observed among promoter single-mutants are consistent with the level of noise in the bulk competition experiment. a,** Selection coefficient measurements for the same genotype typically cover an interval of ~0.028 $gen^{-1}$. The distributions of maximal $|\Delta s|$, the difference between the two most extreme selection coefficient estimates obtained across replicate cultures (n=4), are shown for all assayed single-nucleotide substitutions (Sub; n=462), insertions (Ins; n=462) and deletions (Del; n=96) in the *FCY1* promoter. **b,** The number of mutations exceeding different thresholds of minimal fitness effect is consistent with the expectation derived from random shuffling of the data. Across a range of minimal $|s|$, all genotypes for which the lowest fitness estimate is above $+s$ (significant beneficial effects) or the highest estimate is below $-s$ (significant deleterious effects) are shown (dots). The solid line and shaded area display the median and associated 95% confidence interval for the number of significant effects (using the same definition) obtained from random permutations of the data (n=10 000). Within each iteration, 1020 mock single mutants were assembled by randomly combining selection coefficients from each of the four replicate cultures (Methods). **c,** Twelve promoter single-mutants display $|s| > 0.01$ in the bulk competition experiment. For each genotype, all replicate $s$ estimates are shown (dots). The identifiers of the mutations (x axis) inform on their type (deletion, insertion or substitution), position relative to the *FCY1* coding sequence (where 0 is the base immediately upstream of the gene), and nucleotide change. **d,** The small fitness effects measured are not clearly related to corresponding changes in *FCY1* expression level. For mutants included in panel **c**, the median selection coefficient estimate is compared with Wt-relative expression level estimated from sort-seq (see **Fig. 4e**). Whereas the correlation is negative as expected, the second highest fitness effect is observed for a mutation increasing expression (>1) and the most negative selection coefficient is associated with a moderate decrease of *FCY1* expression.

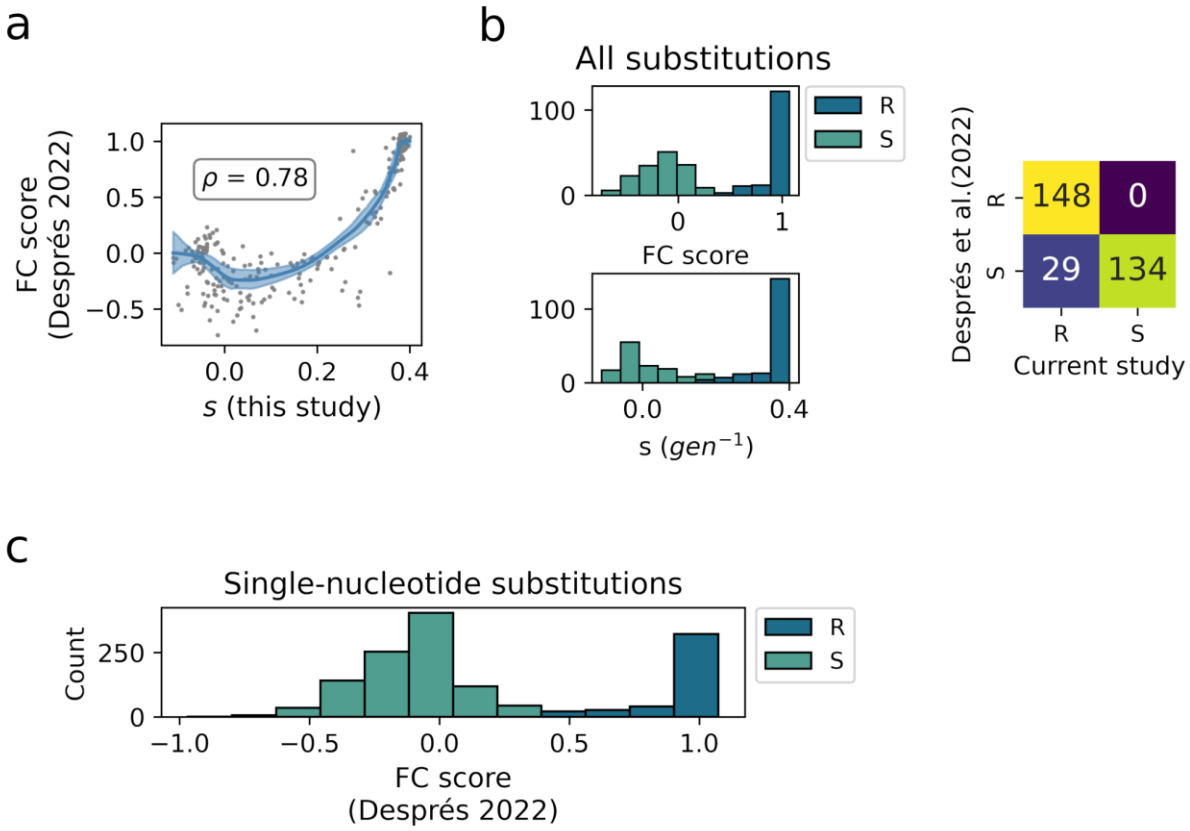


**Extended Data Fig. 5**: Single-nucleotide substitutions in the *FCY1* coding sequence readily confer resistance to 5-FC, across experiments. **a,** Comparison of median selection coefficients for coding sequence mutants (n=960) added to the bulk competition experiment with previously published variant effect scores measured in the same conditions[36]. Values have been aggregated into medians for all genotypes which result in the same amino acid sequence, such that n=311 points are shown. A LOWESS fit highlights a mostly monotonically increasing trend, as shown by a high Spearman correlation ($p < 10^{-64}$). **b,** The set of coding variants which confer resistance to 5-FC is consistent across the two experiments. All mutants which were added to the "+*FCY1*" samples (**Extended Data Fig. 3a**) were classified into resistant (R), and sensitive (S) variants according to their effect in 5-FC conditions, using Gaussian mixture models (*Methods*). This was done using either the FC score reported by[36] (top) or the selection coefficients inferred in the current study (left). The confusion matrix (right) shows that, among all variants which were classified as resistant using data from[36], none appear sensitive to 5-FC in the current study. As in the previous panel, mutated sequences were collapsed into amino acid substitutions resulting in 311 variants. **c,** Almost a third of single-nucleotide substitutions in *FCY1* confer resistance to 5-FC. The distribution of variant effect scores from[36] for all single-nucleotide substitutions in *the coding sequence*. For each genotype (n=1411), the score reported for the corresponding amino acid variant was used. Only 20 of the possible nucleotide substitutions are missing, mostly in the first and last codons. Variants are identified as resistant (R) or susceptible (S) according to the classification shown in panel **b**. The "R" class includes ~29% (408/1411) of the single substitutions shown.

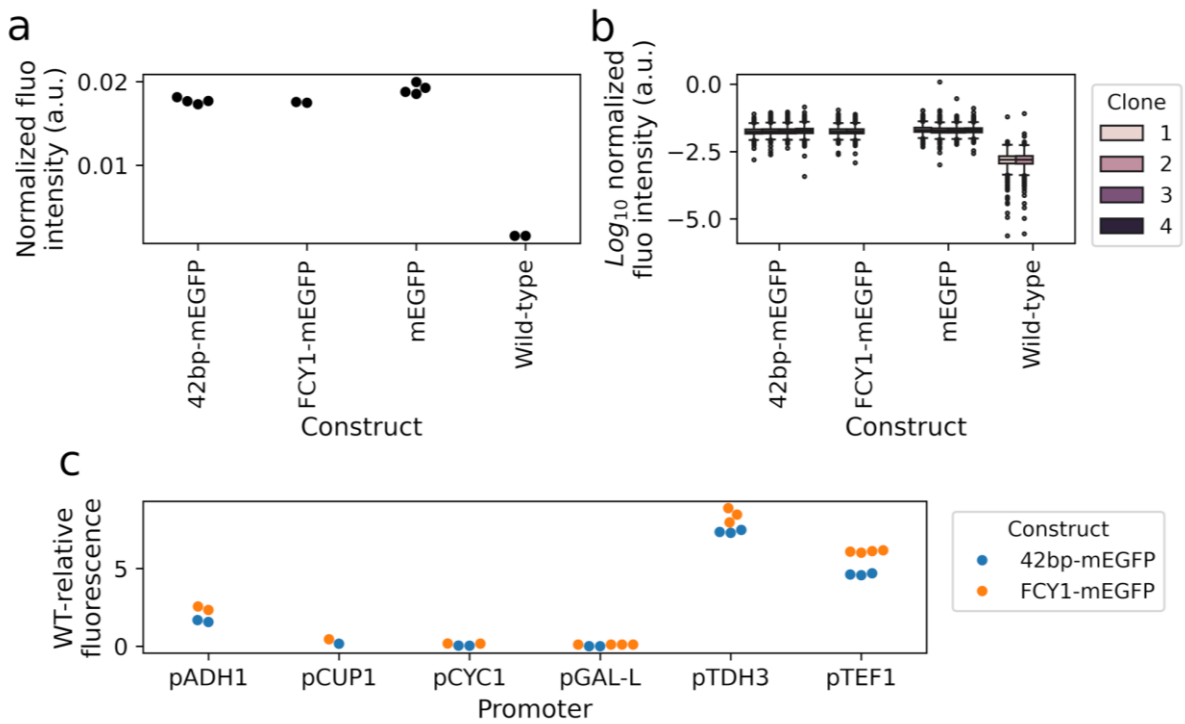


**Extended Data Fig. 6**: **Validation of the 42bp-mEGFP construction. a,** Medians of normalized fluorescence intensity, as measured by flow cytometry (*Methods*), for three mEGFP insertions at the genomic *FCY1* locus. Each point is a distinct clone of the corresponding strain, except for the WT. In the 42bp-mEGFP construct, which was used in the current study to measure promoter activity, the mEGFP green fluorescent protein is fused in C-terminal of the first 42 bp of the *FCY1* coding sequence. In contrast, FCY1-mEGFP designates a C-terminal fusion with full-length *FCY1,* while mEGFP stands for the insertion of the fluorescent protein in place of the *FCY1* coding sequence. **b,** As on the left, but showing the full distribution of log-scaled normalized fluorescence intensities for each clone (5000 events). **c,** Comparisons of median WT-relative fluorescence intensities for the different promoter constructs, in the 42bp-mEGFP or FCY1-mEGFP backgrounds. In each case, the WT-relative value has been computed relative to the corresponding reference (WT *FCY1* promoter sequence, upstream of either the 42bp-mEGFP of FCY1-mEGFP construct). The ranks of the promoters are unchanged between the two backgrounds, although WT-relative fluorescence intensities are consistently higher when the fluorescent protein is fused to full-length *FCY1*. Values shown for the 42bp-mEGFP are the same ones which were used throughout the paper to draw expression-fitness curves, although replicate measurements obtained from the same clone were aggregated into grand medians. The FCY1-mEGFP strains had not been validated prior to cytometry. All clones which displayed a fluorescence intensity clearly different from the corresponding WT are shown. Because the promoter cassettes were directly inserted in place of the endogenous promoter in the WT background, the WT expression level (and thus fluorescence intensity) is expected in cases where integration failed (*Methods*).

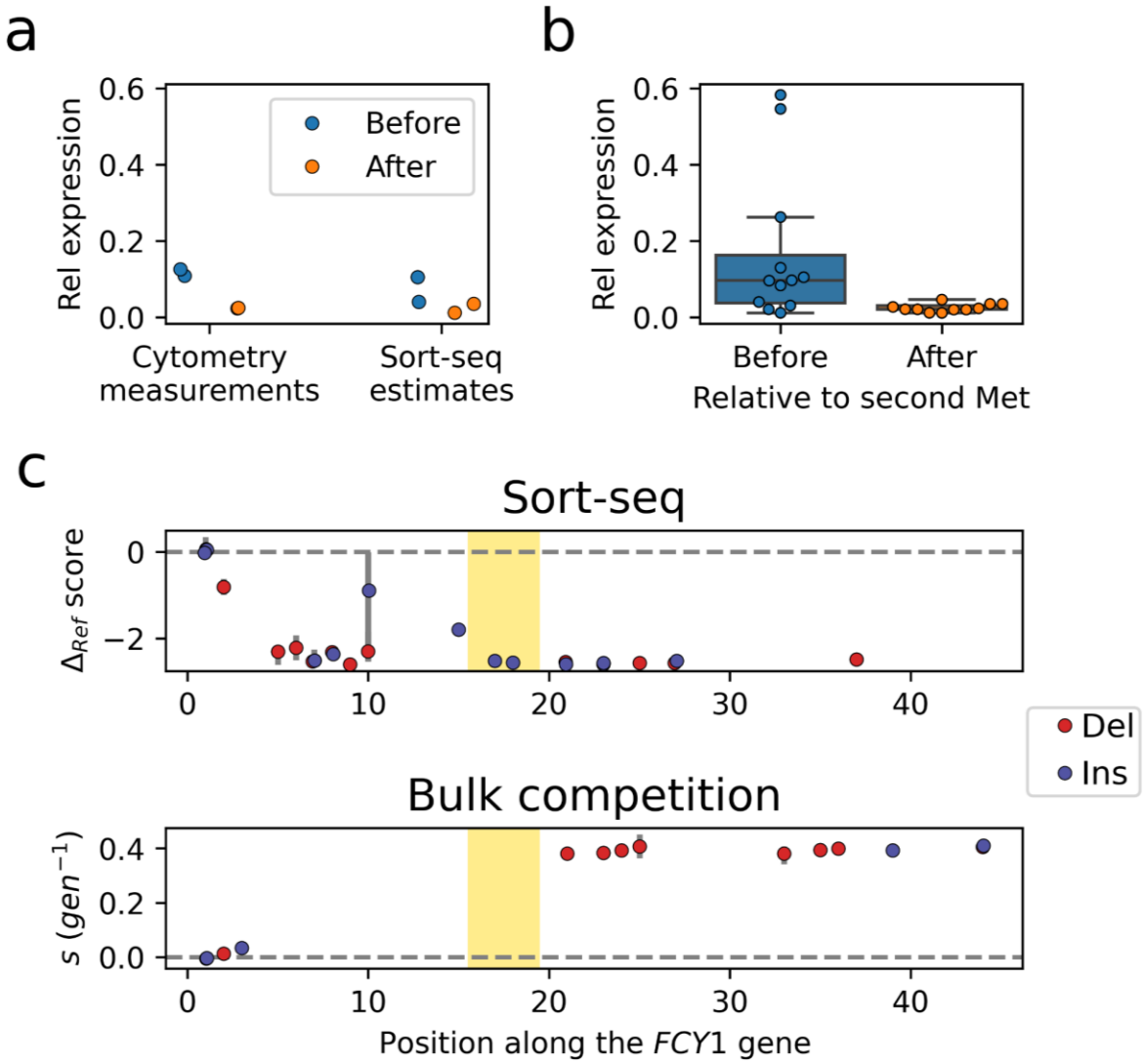


**Extended Data Fig. 7**: **Indels before and after the second methionine codon of *FCY1* have contrasting effects on expression level. a,** Comparison of relative expression levels for the four indel mutations which were included among the set of validation mutations, classified according to whether they occur before or after the second methionine codon of *FCY1*. Cytometry measurements from reconstructed mutants as well as estimates obtained from the large-scale sort-seq experiment are shown. **b,** Relative expression levels, as estimated from the sort-seq experiment, for all detected indel mutations in the *FCY1* coding sequence. Those occurring after the second methionine are clearly more impactful. **c,** Median effect of insertion and deletion variants detected in the sort-seq (top) and bulk competition (bottom) experiments. The shaded area encompasses the three bases of the second methionine codon. Mutations occurring before this codon were recovered at a much lower frequency from the bulk competition, which is consistent with the observation that they do not completely abolish *FCY1* expression and thus do not confer resistance.

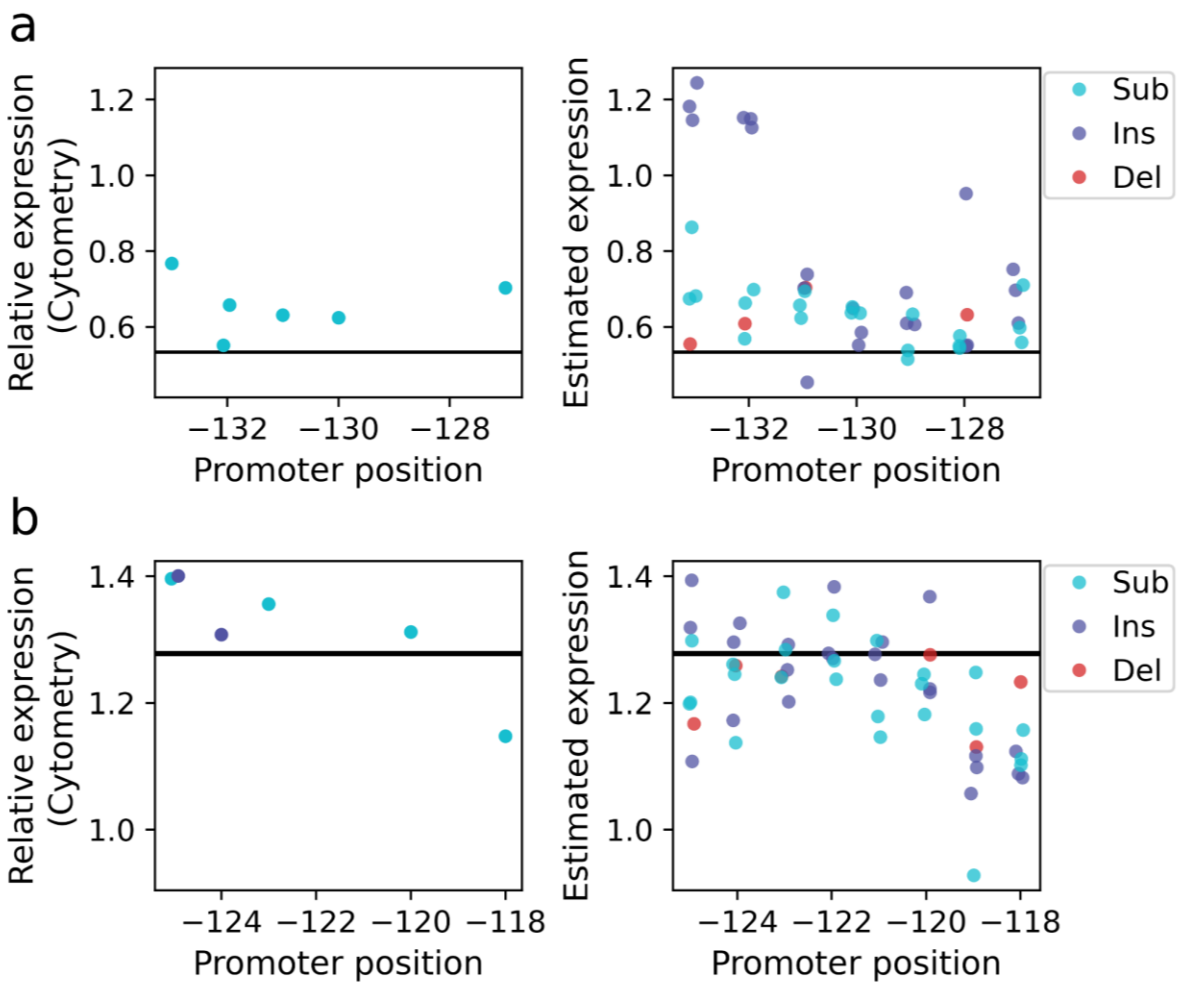


**Extended Data Fig. 8: Deletion of putative TF binding sites is not more impactful than single-nucleotide mutations in the same regions. a,** Deletion of positions -133 to -127 of the *FCY1* promoter, corresponding to site 1 (positions -132 to -127) of **Fig. 4e**. The WT-relative fluorescence of the deletion mutant, from three replicate measurements in flow cytometry, is shown as an horizontal line whose width displays the minimum and maximum values among the three corresponding medians. Among reconstructed validation mutants (left), one single-nucleotide substitution decreases *FCY1* expression as much as the deletion, as shown by its median WT-relative fluorescence intensities (dots; grand median of three replicate cytometry measurements). Among all mutations assayed by sort-seq (right), the most impactful single-nucleotide changes decrease expression as much as the deletion, as shown by the corresponding relative expression level estimates (dots; median of the 95% prediction interval obtained from sort-seq calibration). **b,** Deletion of positions -125 to -118, corresponding to site 2 (-125 to -120) of **Fig. 4e**. The plots are the same as in **a**, but this time for a deletion which increases *FCY1* expression. Cytometry measurements of validation mutants (left) and sort-seq estimates (right) both show that many single-nucleotide changes have an effect that is comparable to that of the deletion – or even larger.

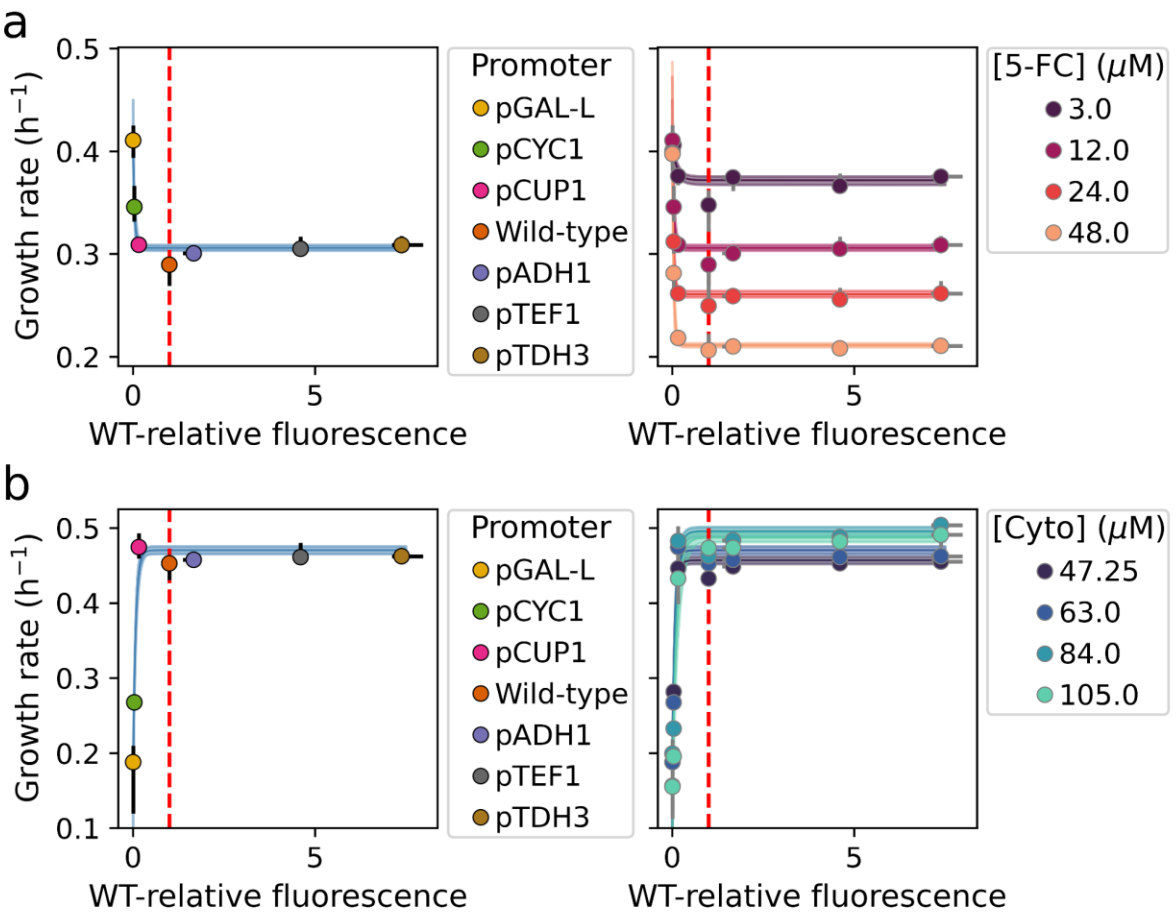


**Extended Data Fig. 9: The insensitivity of fitness to changes in *FCY1* expression level is constant across many concentrations of 5-FC and cytosine. a,** Fitness functions in 5-FC. In [12 μM] 5-FC (left), a constant plateau of low fitness is reached starting from ~0.18 WT-relative expression (same as **Fig. 5b**). Across three additional concentrations of 5-FC (right), the boundary of the plateau does not change. Its height however varies, such that lower growth rates are observed for increasing 5-FC concentrations. **b,** Fitness functions in media lacking uracil, where deamination of cytosine by Fcy1p is essential. When cytosine is added at [63 μM] (left), a similar plateau is observed from ~0.18 WT-relative expression, such that any further increase in *FCY1* expression does not increase growth rate. When three additional concentrations of cytosine are tested (right), the boundary of the fitness plateau also remains constant. Error bars around each dot display minima and maxima of three replicate measurements for growth rate and relative fluorescence intensity for each combination of promoter and 5-FC/cytosine concentration. In addition, dashed vertical lines identify the WT expression level (relative fluorescence intensity of 1.0).

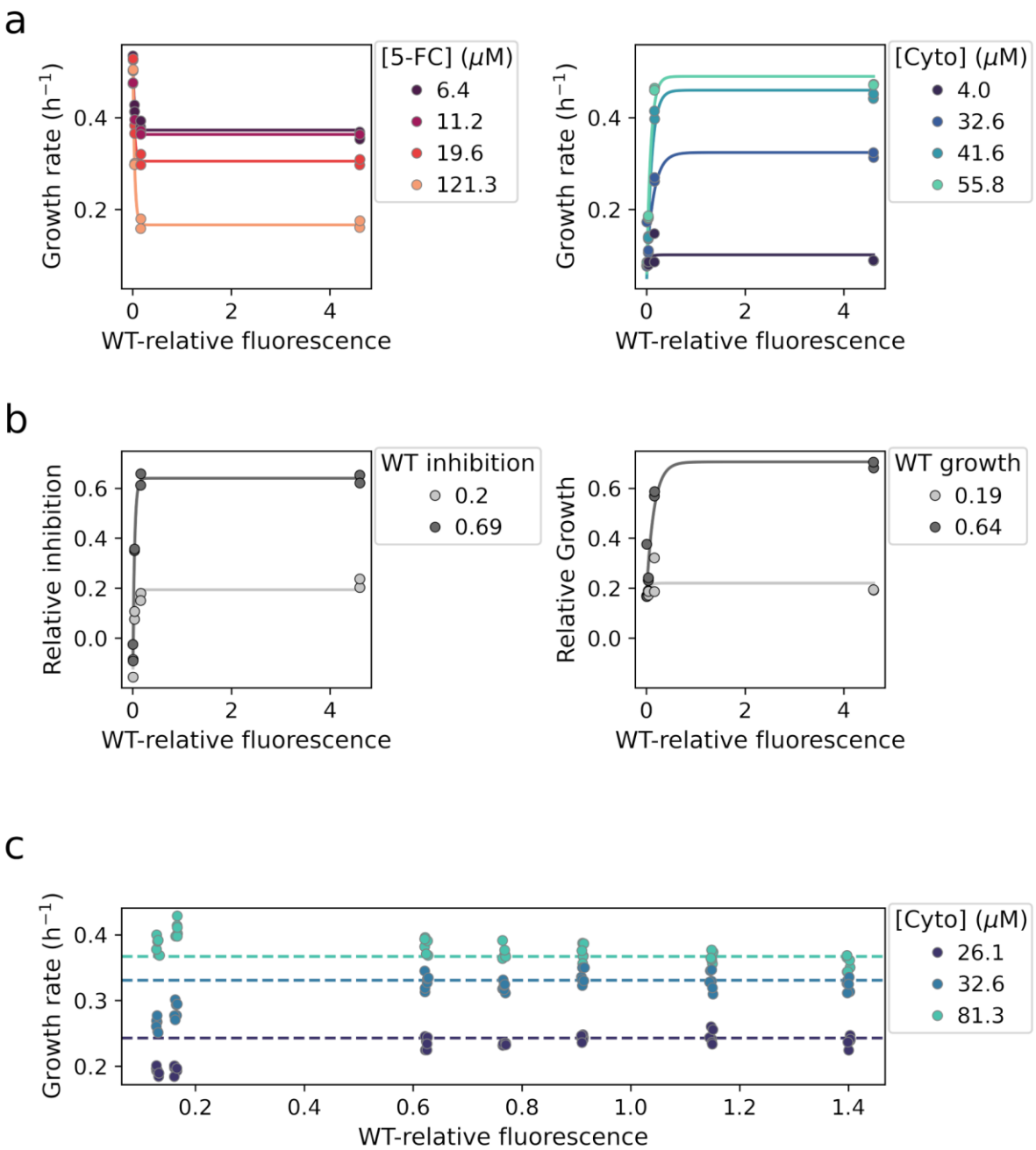


**Extended Data Fig. 10: The expression-fitness function of *FCY1* displays a sign inversion between 5-FC and cytosine conditions. a,** Fitness functions across 5-FC and cytosine concentrations covering the full ranges of the corresponding dose-response curves (**Extended Data Fig. 2**). Exponential growth rate measurements were performed in duplicates for each of the promoter constructs which define the elbow of the fitness function: pGAL-L, pCYC1, pCUP1 and pTEF1. In 5-FC (left), the conditions shown, from the lowest to the highest concentration, respectively result in relative inhibition levels of 0.20, 0.29, 0.40 and 0.69. In cytosine (right), the concentrations shown are respectively associated with the following relative growth levels: 0.19, 0.64, 0.93 and 0.97. **b,** Comparison of fitness functions obtained in 5-FC (left) and cytosine (right**)** concentrations resulting in matching levels of relative inhibition or growth for the WT reference strain (**Extended Data Fig. 2**). Although growth does not reach 0 in cytosine conditions when *FCY1* expression is decreased to very low levels, the two pairs of curves display very similar shapes. Same data as in panel **a**, but converted into relative inhibition or growth values using the relevant dose-response curve. **c,** Increasing *FCY1* expression through single mutations in the promoter does not provide a benefit in cytosine conditions,

1858 where Fcy1 activity is essential for growth. Exponential growth rate measurements were performed in
1859 triplicates for eight reconstructed promoter mutants covering the full range of expression changes
1860 available from single-nucleotide changes (**Fig. 5d**). From the lowest to the highest, the three cytosine
1861 concentrations used respectively result in relative growth levels of 0.42, 0.64 and 0.97. The dashed
1862 horizontal lines display the medians of growth rates obtained for the two mutants closest to the WT
1863 expression level. Across all three concentrations, the mutant associated with the highest expression
1864 level is not clearly fitter than this baseline. This confirms that, just like they are not deleterious in 5-FC
1865 conditions, promoter mutations increasing *FCY1* expression are not beneficial in cytosine conditions.

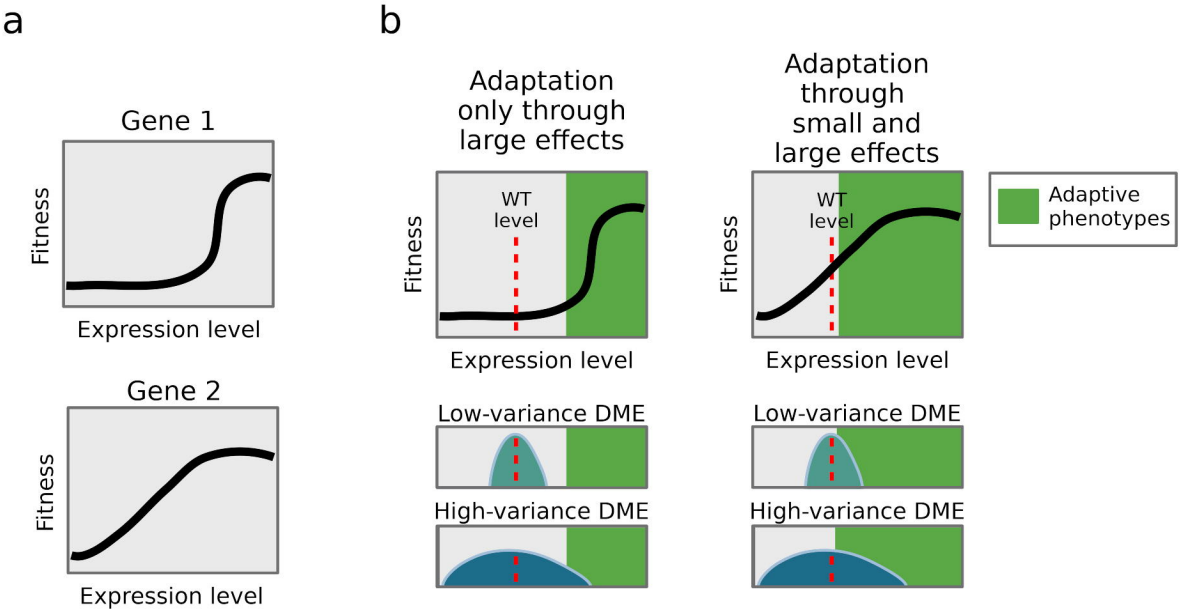
a
Gene 1
Fitness
Expression level
Gene 2
Fitness
Expression level
b
Adaptation only through large effects
Adaptation through small and large effects
WT level
WT level
Fitness
Fitness
Expression level
Expression level
Adaptive phenotypes
Low-variance DME
Low-variance DME
High-variance DME
High-variance DME

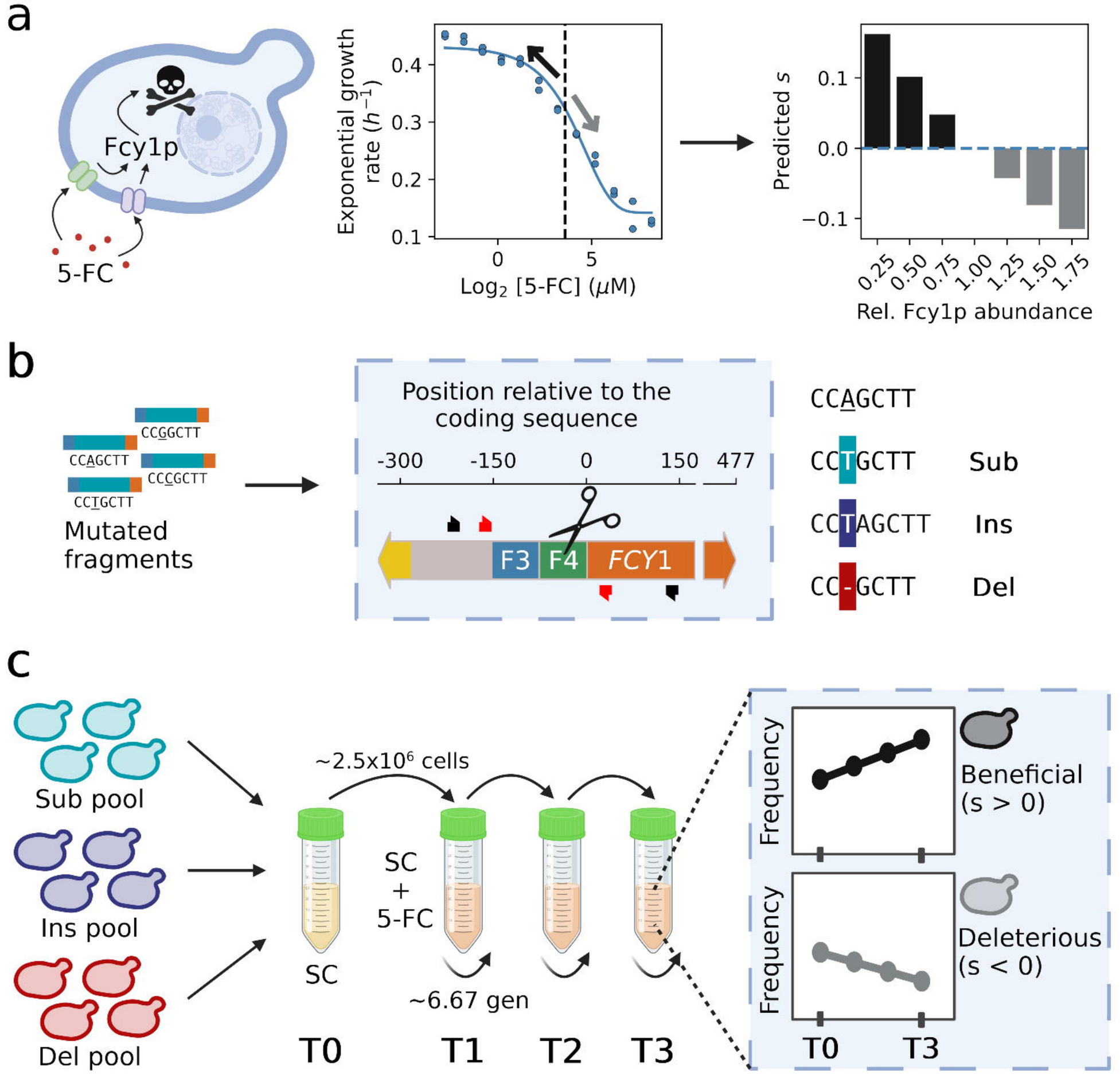
a
Fcy1p
5-FC
Exponential growth rate ($h^{-1}$)
0.4
0.3
0.2
0.1
0
5
$\mathrm{Log}_2$ [5-FC] ($\mu$M)
Predicted $s$
0.1
0.0
−0.1
0.25
0.50
0.75
1.00
1.25
1.50
1.75
Rel. Fcy1p abundance
b
CCGGCTT
CCAGCTT
CCCGCTT
CCTGCTT
Mutated fragments
Position relative to the coding sequence
-300
-150
0
150
477
F3
F4
FCY1
CCAGCTT
CCTGCTT
Sub
CCTAGCTT
Ins
CC-GCTT
Del
c
Sub pool
Ins pool
Del pool
~2.5x10⁶ cells
SC
SC + 5-FC
~6.67 gen
T0
T1
T2
T3
Frequency
Beneficial (s > 0)
Deleterious (s < 0)
T0
T3

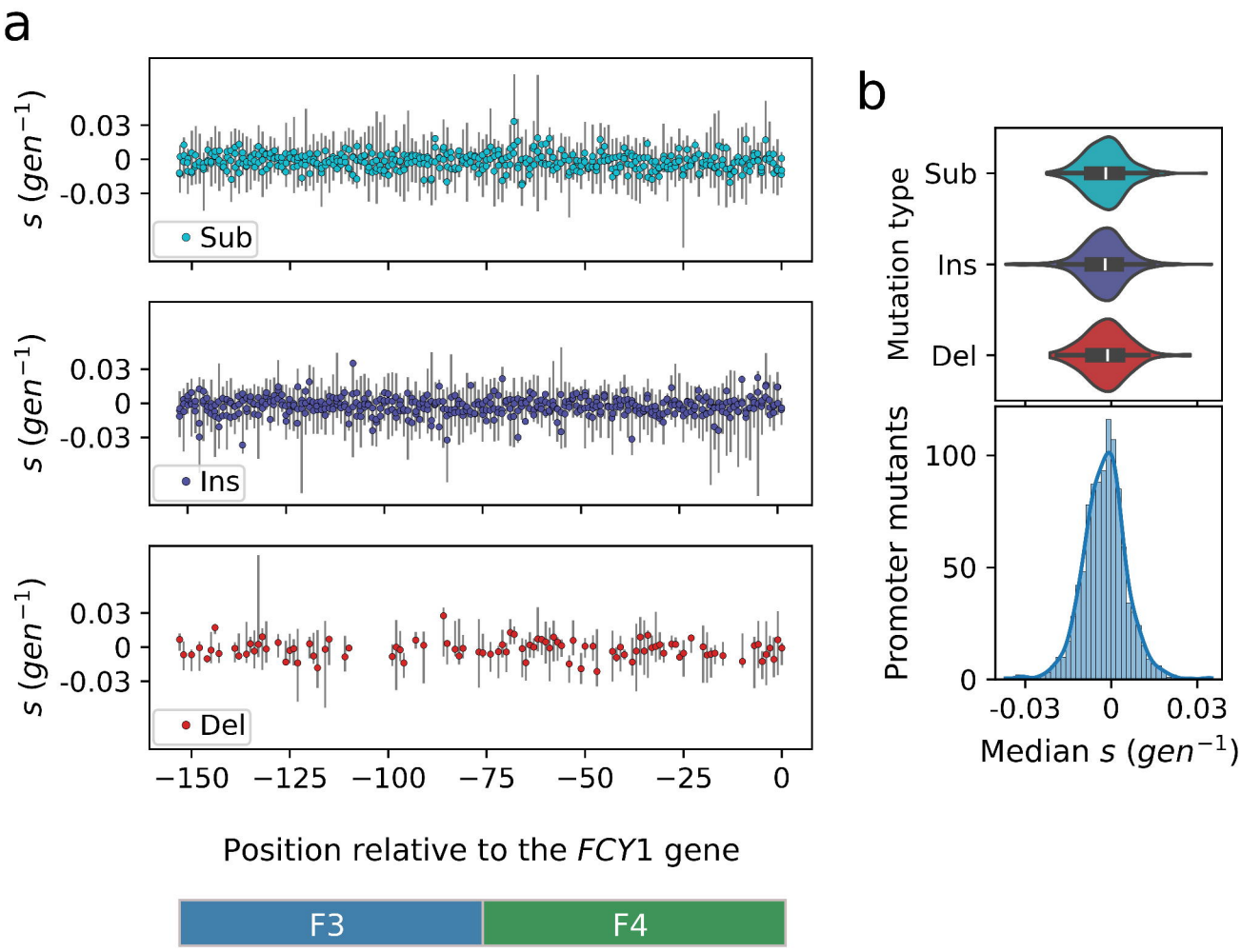
a
b
s (gen$^{-1}$)
0.03
0
-0.03
Sub
Ins
Del
−150
−125
−100
−75
−50
−25
0
Position relative to the FCY1 gene
F3
F4
Mutation type
Promoter mutants
100
50
0
-0.03
0
0.03
Median s (gen$^{-1}$)

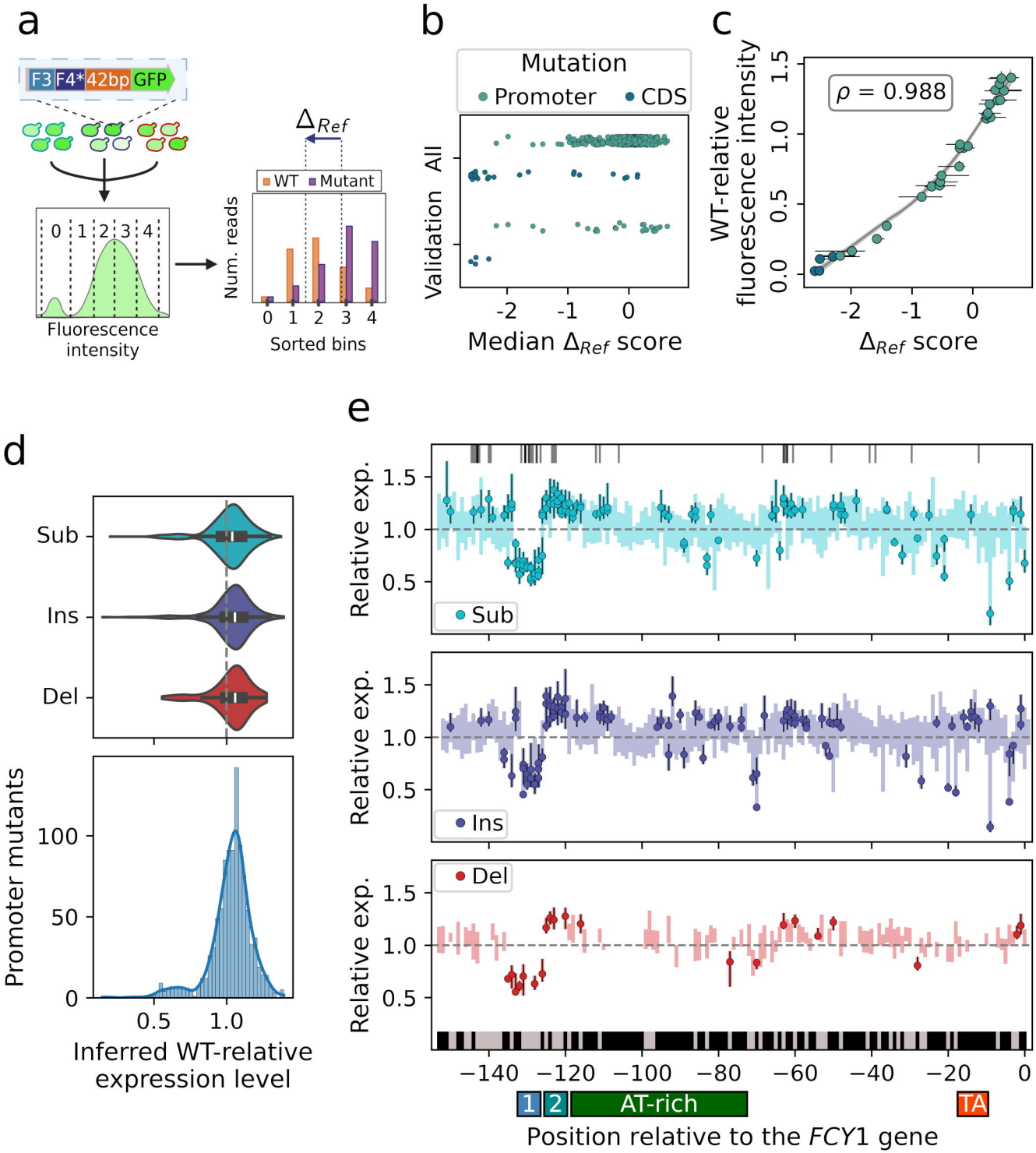
a
F3
F4*
42bp
GFP
0
1
2
3
4
Fluorescence intensity
$\Delta_{Ref}$
WT
Mutant
Num. reads
Sorted bins
b
Mutation
Promoter
CDS
All
Validation
Median $\Delta_{Ref}$ score
c
$\rho$ = 0.988
WT-relative fluorescence intensity
$\Delta_{Ref}$ score
d
Sub
Ins
Del
Promoter mutants
Inferred WT-relative expression level
e
Relative exp.
Sub
Ins
Del
AT-rich
TA
Position relative to the FCY1 gene

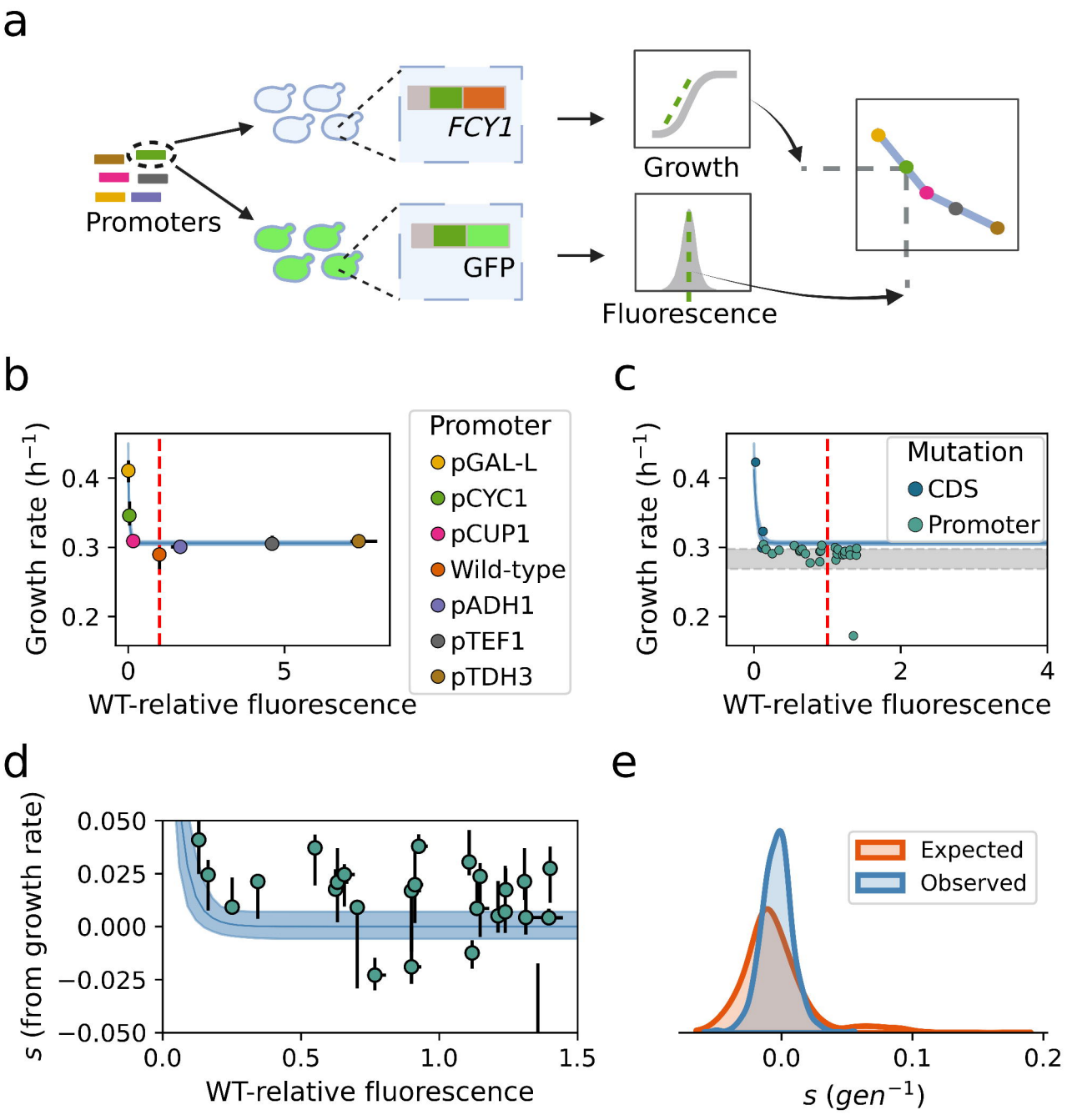
a
Promoters
FCY1
GFP
Growth
Fluorescence
b
Growth rate (h$^{-1}$)
0.4
0.3
0.2
0
5
WT-relative fluorescence
Promoter
pGAL-L
pCYC1
pCUP1
Wild-type
pADH1
pTEF1
pTDH3
c
Growth rate (h$^{-1}$)
0.4
0.3
0.2
0
2
4
WT-relative fluorescence
Mutation
CDS
Promoter
d
s (from growth rate)
0.050
0.025
0.000
−0.025
−0.050
0.0
0.5
1.0
1.5
WT-relative fluorescence
e
Expected
Observed
0.0
0.1
0.2
s (gen$^{-1}$)

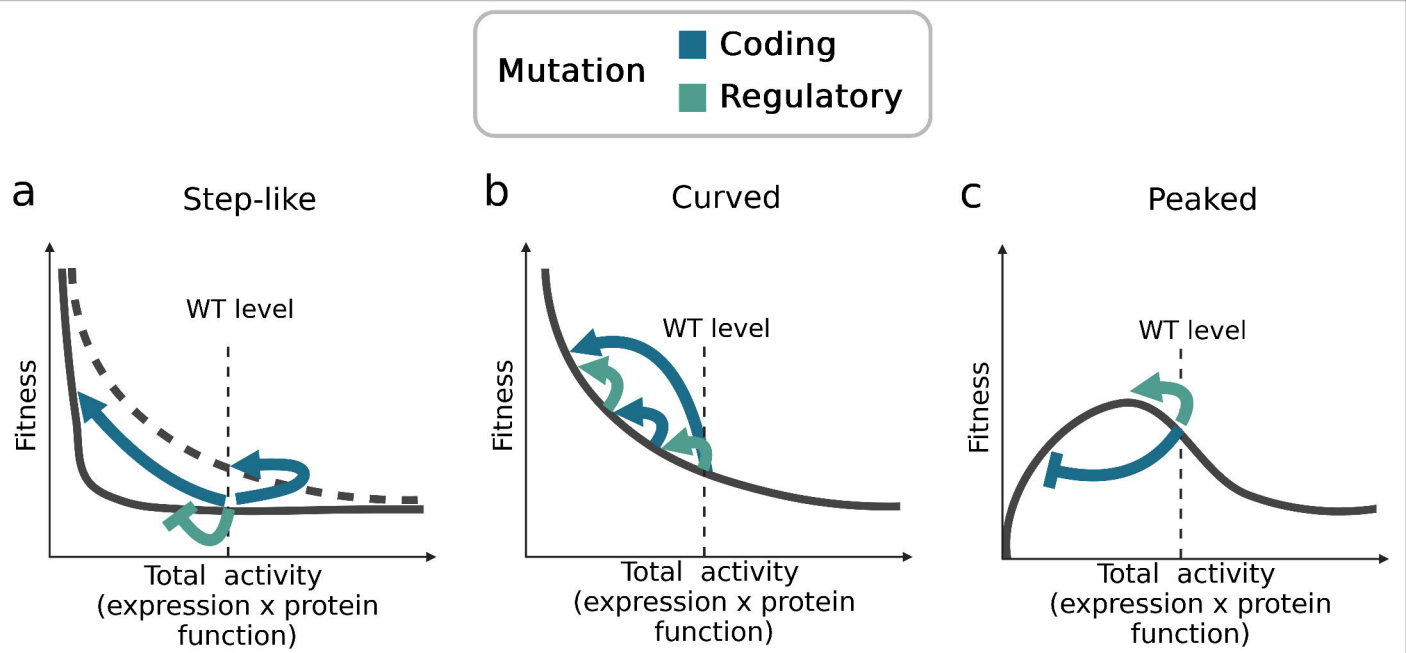
Mutation
Coding
Regulatory
a
Step-like
WT level
Fitness
Total activity
(expression x protein
function)
b
Curved
WT level
Fitness
Total activity
(expression x protein
function)
c
Peaked
WT level
Fitness
Total activity
(expression x protein
function)